UNIVERSIDADE DE LISBOA

FACULDADE DE CIÊNCIAS

DEPARTAMENTO DE BIOLOGIA VEGETAL

Characterization of metabolic pathways involved in the compatible interaction between *Vitis vinifera* and *Plasmopara viticola*

Rui Nascimento

Mestrado em Biologia Molecular e Genética

Dissertação orientada por:

Doutora Marta Sousa Silva

Doutora Andreia Figueiredo

2017

Declaração

De acordo com o disposto no artigo n.º 19 do Regulamento de Estudos de Pós-Graduação da Universidade de Lisboa, Despacho n.º 2950/2015, publicado no Diário da República, 2.ª série — N.º 57 — 23 de março de 2015, foram incluídos nesta dissertação os resultados apresentados em:

Nascimento R., Maia M., Silva M.S., Figueiredo A., Cordeiro C., Ferreira A.E.N.* (2017). **Metabolinks: tools for high-resolution MS metabolomics data analysis.** 5th Portuguese Mass Spectrometry Meeting (PTMS2017), Lisboa - Portugal

Nascimento R.*, Maia M., Ferreira A.E.N., Marques A.P., Ponces Freire A., Cordeiro C., Sousa Silva M., Figueiredo A. (2017). **Metabolic characterization of *V. vinifera* cv. Trincadeira in *Plasmopara viticola* infected leaves.** 5th Portuguese Mass Spectrometry Meeting (PTMS2017), Lisboa - Portugal

Nascimento R.*, Maia M., Ferreira A.E.N., Marques A.P., Ponces Freire A., Cordeiro C., Sousa Silva M., Figueiredo A. (2017). **Metabolic characterization of *V. vinifera* cv. Trincadeira upon *Plasmopara viticola* infection**. Abstract of the CQB DAY 2017 (pp 51), Faculdade de Ciências da Universidade de Lisboa, Lisboa – Portugal.

Nascimento R.*, Maia M., Ferreira A.E.N., Marques A.P., Ponces Freire A., Cordeiro C., Sousa Silva M., Figueiredo A. (2017). **Metabolic characterization of *V. vinifera* cv. Trincadeira in response to *Plasmopara viticola***. 3rd general COST MEETING (COSTFA1306), ITQB, Oeiras – Portugal.

Em cumprimento com o disposto no referido despacho, esclarece-se ser da minha responsabilidade a execução das experiências que estiverem na base dos resultados apresentados (exceto quando referido em contrário), assim como a interpretação e discussão dos mesmos.

Acknowledgements

Este espaço é dedicado àqueles que deram a sua contribuição para que esta dissertação fosse realizada. A todos eles deixo o meu agradecimento sincero.

Em primeiro lugar não posso deixar de agradecer às minhas orientadoras, Doutora Andreia Figueiredo e Doutora Marta Sousa Silva, obrigado pela oportunidade de trabalhar neste projeto que tanto me cativou, por toda a ajuda ao longo do ano, ensinamentos, sugestões, disponibilidade. Muito obrigado.

E sem esquecendo as minhas "co-orientadoras", Marisa Maia e Joana Figueiredo que me também muito me ajudaram, apoiaram e tiveram muita paciência para mim ao longo de todo este ano, um especial obrigado.

Agradeço também ao Doutor António Ferreira por toda ajuda e ensinamentos prestados, ao Doutor Carlos Cordeiro e a todas as pessoas do CQB que me ajudaram neste novo desafio.

À Doutora Anabela Silva por toda a disponibilidade, ajuda, sugestões e paciência que teve comigo.

Obrigado à Faculdade de Ciências da Universidade de Lisboa, ao BioISI e ao Departamento de Biologia Vegetal pela oportunidade.

Um agradecimento aos meus amigos: Gonçalo Laureano, Clemente da Silva e Daniela Ferreira pela companhia e ajuda. Ao Júlio que apesar de este ano estar mais longe, continua sempre presente. E a todos os outros que proporcionaram bons momentos ao longo do ano.

Por fim, mas não menos importante, um muito obrigado à minha família, em especial aos meus pais, ao meu irmão, à minha avó e à minha namorada Olena por todo o apoio e compreensão.

Muito obrigado a todos.

Abstract

Grapevine (*Vitis vinifera* L.) is the most widely cultivated and economically important fruit crop in the world. Last year the total area worldwide under vines crops was 7.5 million hectares, for grape, dried grape and wine production. This reflects a market value over 29 billion euro for the wine industry alone. The domesticated varieties of grapevine are highly susceptible to many fungal infections, of which downy mildew (DM) is one of the most threatening. Downy mildew is caused by the biotrophic oomycete *Plasmopara viticola* (Berk. et Curt.) Berl.et de Toni affecting the leaves, shoots and fruits, reducing berry quality and yield, with significant production losses.

Currently the most widely used strategy for pathogen control is the use of powerful fungicides, in many cases very prejudicial to human health. Another alternative is the development of new hybrid grapevines that combine good berry quality and high degree of resistance, which usually can take upwards of 2-3 years. Having in mind these shortcomings, the investigation of compatible interaction can provide information on the availability of defense mechanism, but also help in the development of new control strategies and possible define alternative control methods.

In the present work, the metabolic characterization of the first 24 hours of infection, regarding the establishment of the compatible interaction between *Vitis vinifera* cv Trincadeira (susceptible cultivar) and *Plasmopara viticola* were characterized. The metabolic changes were characterized by Fourier Transform Ion Cyclotron Resonance MS (FTICR-MS), Gas Chromatography (GC), quantitative real-time PCR (qPCR), and by the quantification of important biological markers, such as ROS, lipid peroxidation and photosynthetic pigments. Our results show that, following inoculation, Carbohydrates and Lipid metabolism reveal pathogen-derived modulation, being lipid variations largely due to Flavonoids and Fatty acids differences. The present study supports the idea that susceptible cultivars try to mount a defense response but are unable to properly respond to the pathogen.

Keywords: *Vitis vinifera*, *Plasmopara vitícola*, compatible interaction, FTICR-MS, metabolic characterization, lipid modulation

Resumo Alargado

A videira (*Vitis vinifera* L.) é a planta de fruto mais cultivada em todo o mundo, devido aos vários produtos de elevada importância económica, em particular o vinho, mas também as uvas, passas de uvas, folhas, entre outros. O ano passado (2016) as plantações de videira a nível mundial cobriam uma área de 7.5 milhões de hectares. Entre os vários produtos que podem ser extraídos ou colhidos das videiras, o vinho é sem dúvida o mais rentável e relevante. Apesar da produção total de vinho não ter crescido significativamente nos últimos anos, a procura tem vindo a impulsionar a indústria vinícola para novos recordes, atingindo um valor de mercado superior aos 29 biliões de euro, um crescimento de aproximadamente de 40% nos últimos 6 anos.

Em Portugal, a videira, também desempenha um papel essencial ao nível da nossa cultura e economia, sendo que o ano passado (2016) as exportações de vinho arrecadaram cerca de 738 milhões de euro. Portugal está entre os 10 maiores produtores de vinho e apresenta a segunda maior variedade de cultivares a nível mundial, numa área de cultivo superior a 190 mil hectares.

No entanto a maioria das variedades utilizadas para o fabrico de vinho são suscetíveis a vários patogénios. Uma das doenças mais ameaçadoras para a produção vitícola no continente europeu é o míldio da videira. Esta doença, causada pelo oomicete obrigatório *Plasmopara viticola* (Berk. et Curt.) Berl. et de Toni, afeta a maioria das castas de *Vitis vinifera* utilizadas para o fabrico de vinho. As infeções por *P. viticola* afetam não só as folhas, mas também os rebentos e os frutos, e têm impactos negativos nas produções de videira, levando a grandes perdas das colheitas e redução da qualidade dos frutos e consequentemente elevados impactos económicos.

Sob condições adequadas, isto é, humidade elevada e temperatura moderada (entre os 22 e 25 °C), os oósporos germinam, dando origem a zoosporângios que libertam zoósporos capazes de aderir à face abaxial das folhas. Uma vez germinados, os zoósporos, entram através dos estomas, para a cavidade estomática, onde se dá o desenvolvimento das hifas primárias e micélio. As hifas e o micélio invadem os espaços intercelulares, levando invariavelmente à invaginação da membrana plasmática das células do parênquima. O micélio também se desenvolve e emerge através do estoma sob a forma de esporangióforos, libertando esporângios que levam a infeções secundárias em tecidos próximos suscetíveis (folhas, ramos, frutos) e ainda a outras plantas.

Atualmente as estratégias de controlo assentam-se no uso de pesticidas e fungicidas, que se podem tornar perigosos para o meio ambiente e para os humanos. Plantações de videiras não

protegidas por qualquer tipo de controle de pragas, arriscam-se a sofrer perdas superiores a 75% da produção anual, o que acarreta custo muito elevados.

As alternativas ao uso de pesticidas recaem na criação de híbridos entre as variedades suscetíveis, que têm grande qualidade de uva e boas propriedades para o fabrico de vinho, e variedades americanas e asiáticas que são tolerantes ou resistentes à infeção. Esta última abordagem é claramente mais eficaz e sustentável, no entanto também traz os seus problemas associados. Cruzamentos de modo a criar híbridos de interesse ou até mesmo a transformação de videiras pode demorar vários anos, o que se tornam processos muito longos e dispendiosos.

Frequentemente a diferença entre uma variedade resistente e uma suscetível é uma questão de amplitude e/ou afinamento da resposta de defesa. Como tal, o estudo de interações compatíveis (suscetível) é tão importante como o estudo de interações incompatíveis (resistentes). Interações compatíveis podem fornecer importantes informações relativas aos diferentes mecanismos de defesa presentes, mas também ajudar no desenvolvimento de novas estratégias de defesa e identificar fatores relevantes na progressão da doença.

Vários estudos têm sido feitos no âmbito de aprofundar o conhecimento destas interações compatíveis e de conhecer melhor como se processa a infeção numa variedade suscetível. De modo a compreender os marcadores genéticos associados à resistência e/ou falta deles, as analises de *Quantitative trait Loci* (QTL) têm sido fundamentais na identificação de múltiplos *loci* de interesse. Até agora 16 *loci* de Resistência de *Plasmopara viticola* (RPVs) foram descritos.

A análise de transcritómica em interações com míldio de videira é frequentemente utilizada quer em larga escala (microarrays e sequenciação de RNA) quer em pequena escala (usando a Reação em Cadeia de Polimerase quantitativa (qPCR)). No caso das interações compatíveis com *P. viticola*, é descrita uma redução dos transcritos de genes relacionados com a fotossíntese, e um aumento insuficiente de genes relacionados com a defesa a patogénicos e reguladores de resposta a estímulos. Em paralelo estudos ao nível da proteómica também têm vindo a elucidar a interação planta-patogénio. Após infeção com *P. viticola,* folhas de cultivares suscetíveis acumulam certas proteínas alergénicas relacionadas com defesa, mas também glicoproteínas associadas na desregulação dos estomas. Apresentam também fosforilação associada a proteínas do metabolismo e fotossíntese. Na área da metabolómica o número de estudos em interações compatíveis entre a videira e o *P. viticola* são reduzidos. Em trabalhos anteriores utilizando ressonância nuclear magnética de protão (H^1NMR), identificámos um

número reduzido de metabolitos modulados em *V. vinífera* cv Trincadeira pela interação com o *P. viticola.*

No âmbito deste trabalho, a caracterização metabólica das primeiras horas da interação compatível, entre a variedade suscetível Trincadeira com o *P. viticola,* foi realizada por espectrometria de massa de ressonância ciclotrónica de iões com transformada de Fourier (FTICR-MS). Esta técnica apresenta uma elevada sensibilidade de poder de resolução permitindo uma caracterização metabólica mais detalhada. Os resultados obtidos, após a inoculação, sugerem modelação lipídica tal como do metabolismo dos carboidratos, de modo que análises complementares foram realizadas de modo a melhor caracterizar estes processos. Análise por Cromatografia gasosa revelou diferenças nos principais ácidos gordos em folhas infetadas, do mesmo modo que as análises por qPCR revelaram modulação nas vias dos Flavonoides. A quantificação dos açucares nas folhas também revelou diferenças no conteúdo de carboidratos.

Estes dados sugerem que as variedades suscetíveis tentam iniciar um processo de defesa, mas esta não é robusta o suficiente para impedir o desenvolvimento do *P. viticola*, acabando por se dar inicio à infeção.

Palavras Chave: *Vitis vinifera*, *Plasmopara vitícola*, interação compatível, FTICR-MS, caracterização metabólica, modulação dos lípidos

Table of Contents

List of Figures:

List of Tables

List of equations

Abbreviations

°C	Celcius
Abs	absorbance
ANR	Anthocyanidin reductase
cDNA	complementary DNA
cv.	cultivar
DBI	double bond index
DGDG	Di–galactosyldiacylglycerols
DM	Downy mildew
DNS	Dinitrosalicylic Acid
DW	Dried weight
EF1α	*Elongation factor 1-alpha*
ESI	Electrospray Ionisation
F3'5'H	*Flavonoid 3',5'-hydroxylase*
FA	Fatty Acids
FatB	*Fatty acyl-ACP thioesterase B*
FLS	*Flavonol Synthase/Flavanone 3-hydroxylase*
FTICR-MS	Fourier Transform Ion Cyclotron Resonance MS
FW	Fresh weight
g	Centrifuge force
g	gram
GC	Gas Chromatography
h	hour
hpi	hours post-infection
LAR2	*Leucoanthocyanidin reductase 2*
m/z	mass to charge ratio (Unit: Thomson)
mg	miligram
MGDG	Mono–galactosyldiacylglycerols
ml	milliliter
MS	Mass Spectrometry
NSC	Non-Structural Carbohydrates
P. viticola	*Plasmopara viticola*
PA	phosphatidic acid

PC	Phosphatidylcholine
PCR	Polymerase Chain Reaction
PE	phosphatidylethanolamine
PG	phosphatidilglycerol
PI	phosphatidylinositol
PLS-DA	projection to latent structures discriminant analysis
PR	Pathogenesis-related
qPCR	quantitative real-time PCR
ROS	Reactive Oxygen Species
SAND	*SAND family protein*
TAG	triacylglycerol
TLC	Thin Layer Chromatography
TS	Total Sugars
TSS	Total Soluble Sugars
v/v/v	Volume/Volume/Volume
w/v	weight/volume
µg	microgram
µmol	micromol

1. Introduction

Grapevine (*Vitis vinifera* L.) is the most widely cultivated and economically important fruit crop in the world, with deep ties to human culture dated to more than 5000 years[1]. Today the wine industry plays a key role in many countries economy, with a global market size of over 29 billion euro[2]. Portugal is the country with the second largest varieties of grapevine cultivars, similarly the wine industry is of crucial importance to our economy. However, most of grapevine cultivars used for winegrowing are often affected by fungal pathogens causing severe harvest losses. One of these diseases, commonly known as downy mildew, is caused by the obligate biotrophic oomycete *Plasmopara viticola* (Berk. et Curt.) Berl. et de Toni, unintentionally introduced into Europe in the late 19th century[3]. With adequate climate conditions, i.e. high humidity and moderate temperatures, *Plasmopara viticola* (*P. viticola*) mature sporangia releases zoospores that are able to place on the abaxial surface of leaves. Then germinate and penetrate the stomatal cavity forming a substomatal vesicle, which in part gives rise to the primary hyphae and mycelium. The hyphae and mycelium invade the intercellular spaces, ultimately leading to the invagination of the plasma membrane of the parenchyma cells causing the oil spots. The mycelium also develops to form sporangiophores emerging from the stoma and releasing sporangia to the surrounding susceptible tissues (leaves, twigs or grape clusters) and other plants[3,4] (Figure 1).

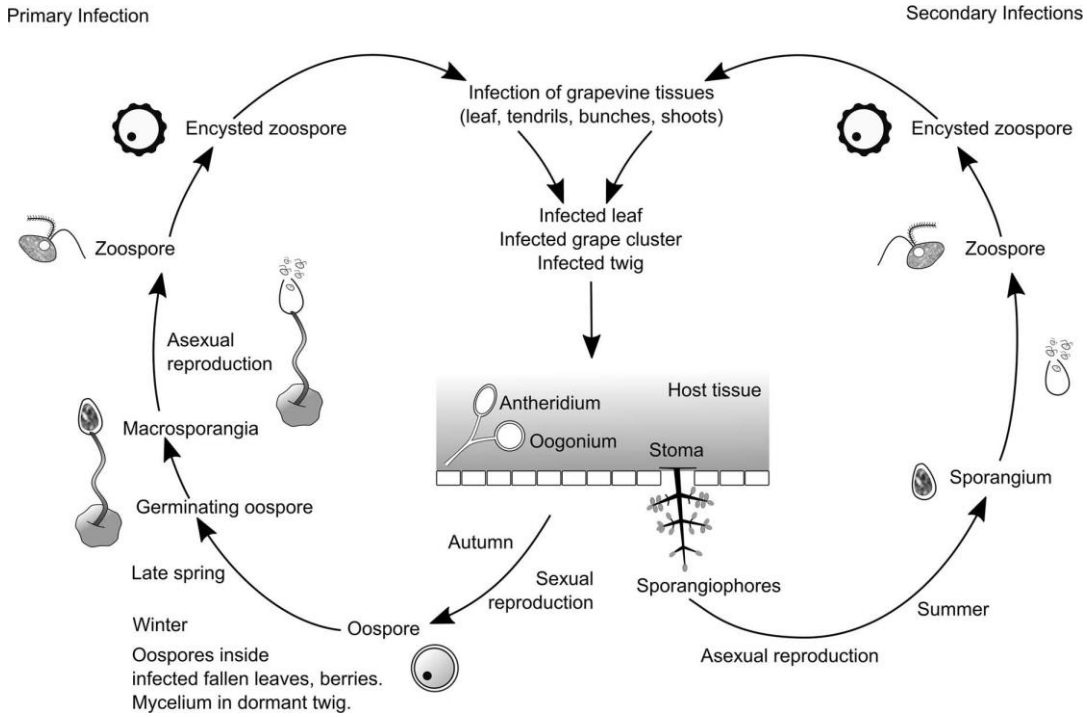

Figure 1 – *Plasmopara viticola* life cycle.

Adapted from Buonassisi et al., 2017[4].

As a result, *P. viticola* can have devastating effects on unprotected crops, reducing the grape quality and can easily destroy up to 75% of production in a single season leading to massive economic losses [3–7].

Frequently the difference between a resistant and susceptible plant is just a question of timing and amplitude of the adequate defense response[8], the knowledge on compatible interactions may provide information on the availability of defense mechanisms, but also aid in the development of new control strategies and possible lead to the identification of pathogen and host factors needed for disease progression[9]. In order to elucidate the *P. viticola* compatible interaction with grapevine, several OMIC studies have been published[9–14].

Generally, a grapevine-*P. viticola* compatible interaction is characterized by a global downregulation of photosynthesis-related processes and inadequate upregulation of genes encoding pathogenesis-related (PR) proteins, enzymes of phenylpropanoid pathways and regulators of response to stimuli[9,15–17].

Along with gene expression analyses, proteomic studies also enlighten the plant–pathogen interaction mechanism. Susceptible grapevine leaves accumulated allergenic defense-related proteins (PR-2 and b-1,3-glucanases)[18] and two glycoproteins implicated in the DM-induced deregulation of stomata during compatible interactions[19]. Compatible interaction is correspondingly associated to phosphorylation of photosynthesis and metabolism related proteins[20].The susceptibility of *Vitis vinifera* to downy mildew suggests that this species lacks a *P. viticola*-specific recognition system that enables the activation of a successful defense mechanism[21]. Nevertheless, both transcriptional, proteomic and metabolomic changes suggest that an early activation of defense processes occurs although it appears to be insufficient to restrain the pathogen growth[8,10,22–26].

In this study, we intend to characterize the metabolic modulation in the early events related to the establishment of a compatible interaction between *Vitis vinifera* cv Trincadeira and *Plasmopara viticola*. Despite metabolomics being a widely used tool for the identification and analysis of the spatial and temporal distribution of metabolites[27,28], metabolomic data on *Vitis vinifera – P. viticola* compatible interactions is scarce. The metabolome modulation at the first hours of the infection process is poorly characterized and only few studies have been published so far[13]. Thus, we have monitored the metabolome alterations by direct infusion Fourier-transform ion cyclotron resonance mass spectrometry (FTICR-MS) and performed a lipid analysis by Gas Chromatography (GC) and thin layer chromatography (TLC). Through a

pathway analysis we have further established important metabolic groups and pathways that were further validated by both biochemical and expression analysis.

2. Objetives

- Analysis and characterization of metabolic variations in the compatible interaction between *Vitis vinifera* cultivar (cv.) Trincadeira and *Plasmopora viticola* at early inoculation time-points (6, 12 and 24 hours post-infection(hpi));
- Comparison of different metabolic profiles from infected and non-infected leaves;
- Pathway analysis of differently accumulated metabolites in order to find the respective coding enzymes;
- Identification of important metabolic groups and pathways in the compatible interaction.

3. Materials and Methods

3.1. Inoculation Experiments

P. viticola inoculations were made in greenhouse grown *Vitis vinifera* cv Trincadeira plants, as previously described[23]. Briefly, *P. viticola* sporangia were collected from symptomatic leaves from greenhouse infected plants after an overnight incubation in a moist chamber at room temperature. Sporangia were carefully collected by brushing, dried and stored at −25 °C. Their vitality was checked by microscopy[29]. A suspension containing 10^4 sporangia ml^{-1} was used to spray the abaxial leaf surface while controls were made by spraying the leaves with water (mock inoculations). After inoculation, plants were kept for 8 h in a moist chamber (100% humidity) and then kept under greenhouse conditions during the inoculation time course. The third to fifth fully expanded leaves below the shoot apex were collected at 6, 12, and 24 hpi, immediately frozen in liquid nitrogen and stored at −80°C. Three independent biological replicates were collected for each condition (inoculated and mock inoculated).

3.2. Metabolite Extraction

Metabolite extraction from inoculated and mock inoculated grapevine leaves was adapted from a previous method[30]. Briefly, metabolites were extracted using a solvent mixture methanol/water/leucine enkephalin solution (2:1:1, v:v) in a ratio of 0.1 g of ground plant material to solvent. Samples were added methanol and water, vortexed by 1 min, then the leucine enkephalin solution was added, after vortexing again for 1 minute, samples were maintained in an orbital shaker for 15 minutes at room temperature. Samples were centrifuged at 1000 *g* for 10 minutes and the supernatant was collected. Samples were immediately processed for analysis.

A final concentration of 0.25 µg/mL was attained for the standard, leucine enkephalin (YGGFL, Sigma Aldrich). This peptide was used for quality control and internal calibration, and the following molecular masses were considered for analysis: $[M+H]^+ = 556.276575$ Da and $[M-H]^- = 554.2620221$ Da.

3.3. Untargeted metabolomic analysis by FTICR-MS

For each sample, the extracted methanol faction was diluted one thousand- fold in methanol for analysis by direct infusion FTICR-MS, using electrospray ionization (ESI) in positive (ESI^+) and negative (ESI^-) modes [30]. Formic acid (0.1% (v/v), Sigma Aldrich, MS grade) was added

to all samples analysed in ESI^+, for the purpose of aiding with the ionization method. Metabolite analysis was performed by direct infusion in the actively shielded 7-Tesla Apex Qe Fourier Transform Ion Cyclotron Resonance Mass Spectrometer (FTICR-MS, Brüker Daltonics). The Electrospray Ionisation (ESI) source conditions in positive ion mode were the following: the capillary voltage was 4.5 kV and in the spray shield was 4.0 kV, the nebulizer gas flow was 2.0 L/min and the transfer capillary temperature was 180 °C. In negative ion mode, ESI source conditions were: capillary voltage was 4.3 kV and in the spray shield was 3.8 kV, the nebulizer gas flow was set to 2.5 L/min and the transfer capillary temperature was 220 °C. Ions were accumulated in source for 0.1 s and in the collision cell for 1.0 s; time-of-flight was 0.0010 s. Mass spectra were acquired by accumulating 50 scans of time-domain transient signals in 512k-point time-domain data sets. The estimated resolving power is 32000 at m/z 400, with a mass accuracy better than 2 ppm with external calibration and better than 1 ppm with internal calibration (using the standard leucine enkephalin). Mass spectra were recorded in the mass range between 100 and 1000 m/z.

3.4. FTICR-MS spectra and data analysis

The software package Data Analysis 4.1 (Brüker Daltonics, Bremen, Germany) was used to analyse and internally calibrate the mass spectra (using the leucine enkephalin standard and the single-point calibration tool in the software). Mass peak lists were exported with isotopic deconvolution as ASCII files, with a signal-to-noise ratio of 4. The alignment of the three biological replicates was performed using an in-house developed Python-based script by combining the peak lists to a peak matrix considering an error of 1.0 ppm, as previously described [30]. For metabolite identification, the final mass list was uploaded to MassTRIX 3[31] server (http://masstrix.org, accessed in April 2017) considering the following parameters: scan mode was positive or negative ionization; for the data obtained in positive ionization mode the adducts $M+H^+$, $M+K^+$ and $M+Na^+$ were considered; for negative ionization mode data, were selected the adducts $M-H^+$ and $M+Cl^-$; a maximum m/z deviation of 2 ppm; the organism *Vitis vinifera* was selected; the search was performed using the option "KEGG/HMDB/LipidMaps without isotopes". Class separation and differentially accumulated metabolites discrimination were accessed following the MetaboAnalyst 3.0[32], a web-based comprehensive tool suite for metabolomic data analysis (http://www.metaboanalyst.ca) workflow. The intensities of the annotated mass list were normalized using the intensity of leucine enkephalin (556.276575 mass ($M+H^+$) for ESI^+ and 554.2620221 mass ($M-H^+$) for ESI^-). Data was used for multivariate

analysis technique by projection to latent structures discriminant analysis (PLS-DA) to view the class discrimination using score plot and the important masses contributing to the variation were obtained from the loading plot values. Obtained data were validated by t-test ($p \leq 0.05$).

3.5. Compound Classification

Compounds were classified using the KEGG[33,34] (Kyoto Encyclopedia of Genes and Genomes, http://www.genome.jp/kegg/) database classification, except lipids, for which the LIPID MAPS[35] (Lipidomics Gateway, http://www.lipidmaps.org/) classification was considered. For each mass, an initial conversion of HMDB to KEGG identifiers was performed using the "Linked entries option" option in the KEGG REST Service (http://rest.genome.jp/link/compound/hmdb). For lipid annotation, KEGG identifiers with LIPID MAPS correspondence were converted also using the using the "Linked entries option" (http://rest.genome.jp/link/compound/lipidmaps). Metabolite annotation into classes was performed by an in-house Python-based script, which uses the REST services of KEGG and LIPID MAPS Structure Database, using the KEGG and the LIPID MAPS identifiers as input, respectively. Finally a LIPID MAPS to KEGG conversion was performed and all KEGG identifiers containing KNApSAcK[36] (A Comprehensive Species-Metabolite Relationship Database, http://kanaya.naist.jp/KNApSAcK/) equivalencies were searched for their presence in the Plantae Kingdom. For masses with multiple annotations a manual curation was performed. A schematic diagram showing the analysis pipeline is presented in Appendix 1 and the annotation from all cultivars are presented in Appendix 2.

3.6. RNA Extraction and cDNA Synthesis

Total RNA was isolated from inoculated and mock inoculated samples using the Spectrum™ Plant Total RNA Kit (Sigma-Aldrich, USA) and the residual genomic DNA was hydrolysed with the On-Column DNase I Digestion Set (Sigma-Aldrich, USA) as indicated by the manufacturer. RNA concentration and purity were determined at 260/280 nm using a NanoDrop-1000 spectrophotometer (Thermo Scientific), while its integrity was analysed by agarose gel electrophoresis. Prior to complementary DNA (cDNA) synthesis, all samples were analysed for genomic DNA contamination by a quantitative real time Polymerase Chain Reaction (qPCR) of a reference gene on crude RNA[37]. Complementary DNA (cDNA) was synthesized from 2.5 µg of total RNA using RevertAid®H Minus Reverse Transcriptase

(Fermentas, Ontario, Canada) anchored with Oligo(dT)$_{23}$ primer (Fermentas, Ontario, Canada), following the manufacturer's instructions.

3.7. Quantitative Real Time PCR

Based on the detected compounds, metabolic pathways were identified using the KEGG identifiers submitted to KEGG Mapper – Search & Color Pathway (http://www.kegg.jp/kegg/tool/map_pathway2.html). The selection of genes for qPCR analysis was based on the biochemical pathways relevant for the grapevine defence response and on the differentially detected compounds. *Lipoyl Synthase* (*LipA*, lipoic acid biosythesis), *Flavonol Synthase/Flavanone 3-hydroxylase* gene family (*FLS A, B, C, D, E* and *F*), *Flavonoid-3,5'-hydroxylase* (*F3´5´H*) and *Dihydroflavonol Reductase* (*DFR*) coding genes were selected for expression analysis (Table 1). Moreover, genes related to the biosynthesis of Catechin (*Leucoanthocyanidin reductase 2* (*LAR2*)), Epicatechin (*Anthocyanidin reductase* (*ARN*)) and Hexadecenoic acid (*Palmitoyl-acyl carrier protein thioesterase* (*FatB*)) were also included in the analysis (Table 1).

qPCR experiments were performed using the Maxima™ SYBR Green qPCR Master Mix (2×) kit (Fermentas, Ontario, Canada) following manufacturer's instructions. Each set of reactions included a control without cDNA template. Reactions were performed in the StepOne™ Real-Time PCR system (Applied Biosystems, Sourceforge, USA).

For all genes, thermal cycling started with a 95 °C denaturation step for 10 minutes followed by 40 cycles of denaturation at 95 °C for 15 seconds and annealing for 30 seconds. Dissociation curve analysis was performed to confirm single product amplification and the existence of non-specific PCR products (Appendix 3). Three biological replicates and two technical replicates were used for each sample. Gene expression (fold change) was calculated as described in Hellemans et al. 2007[38]. *Elongation Factor 1-alpha* (*EF1α*), Tetratricopeptide *repeat protein 7B** (*TPR7B*) and *SAND family* (*SAND*) were used for expression data normalization as previously described[39].

Table 1 - Candidate reference genes and target genes transcripts primer sequences, amplicon length and qPCR analysis.
EF1α, TPR7B and *SAND* were used as reference genes. *FLS-B* and *FLS-C* were not detected in inoculated samples. *This sequence corresponds to the sequence SMD3 previously described in Monteiro et al., 2013[39]. **Splicing variants.

Enzyme	Abbreviation	NCBI Accession Number	Primer Sequence	Amplicon length (bp)	Ta (°C)	Tm (°C)
Elongation Factor 1-alpha	*EF1α*	XM_002284888.2	Fw: GAACTGGGTGCTTGATAGGC Rev: ACCAAAATATCCGGAGTAAAAGA	149	60	79.4
Tetratricopeptide repeat protein 7B*	*TPR7B*	XM_002283371.4	Fw: GCTCTGTTGTTGAAGATGGG Rev: GGAAGCAGTTTGTAGCATCAG	156	60	79.5
SAND family	*SAND*	XM_002285134.3	Fw: CAACATCCTTTACCCATTGACAGA Rev: GCATTTGATCCACTTGCAGATAAG	76	60	78.5
Leucoanthocyanidin reductase 2	*LAR2*	AJ865334	Fw: TGTAACCGTGGAAGAAGATGA Rev: ATGAAGATGTCGTGAGTGAAG	92	60	80.2
Anthocyanidin reductase	*ANR*	BN000166	Fw: ATCAAGCCAGCAATTCAAGGA Rev: CAGCTGCAGAGGATGTCAAA	93	60	76.3
palmitoyl-acyl carrier protein thioesterase	*FatB*	XM_002284814	Fw: TCGCAAACCCTAGAAACCAAT Rev: AATGAGGGAAGGAGGAAAATG	112	60	77.5
Lipoyl Synthase (chloroplastic)	*LipA*	XM_002270044.4 XM_019222434.1	Fw: ACCCCACCAAAATCATCCTCA Rev: ACAATTCGCAAGCCCCAACT	71	60	76.2
Flavonol Synthase/ Flavanone 3-hydroxylase	*FLS-A*	XM_002264771.4	Fw: TTACAAGAGCGTGGAGCATC Rev: AGCCGGTTCAATGAGCAAAT	103	60	78.8
	FLS-B	XM_002284377.4	Fw: ACAATGGCGGTAGAGAGAGT Rev: TGGGGACTTGAGGGATACAC	Not detected in inoculated samples		
	FLS-C	XM_002285802.3	Fw: TGGTGGTAGGCGATAATGGA Rev: ATGAAGGGTTGTGATGGCAG	Not detected in inoculated samples		
	FLS-D	XM_002285803.4	Fw: AAGCCCAAACCCAAGACAAC Rev: TGAACTCGGGAGGGATGATG	124	60	79
	FLS-E	XM_002285805.3	Fw: AGGAGTACAGTGGACAAGGA Rev: GGTAGCGGTACTCAGCAAAG	151	60	80.8
	FLS-F	XM_002272959.3** XM_019223988.1**	Fw: CTCCGCATGCCTTCATAGTC Rev: ATCGCTCTTCGGGTTGTAGA	143	60	78.4
Flavonoid-3,5'-hydroxylase	*F3'5'H*	NM_001281228	Fw: GCAAAGATGGCCAAAAGATAC Rev: GGCGGGCGGTTAGAGAAAT	134	60	81.1
Dihydroflavonol Reductase	*DFR*	NM_001281215.1	Fw: CCGTTCGCGATCCAACTAAC Rev: CATCGAAACTTCCTTCATCAG	114	60	79.3

3.8. Lipid analysis

The analysis of Gas Chromatography and Thin Layer Chromatography were realized in scope of **Gonçalo Laureano** master thesis, entitled "**Fatty acids and lipid signaling in grapevine resistance to *Plasmopara viticola***".

Frozen ground leaves were boiled in water for 5 min to inactivate lipolytic enzymes. The extraction of lipophilic compounds was performed using a mixture of chloroform/methanol/water (1:1:1, v/v/v), as previously described[40]. Lipid classes' separation was carried out at 6 hpi by thin layer chromatography (TLC) on silica plates (G-60, Merck, VWR), as previously described[41] using a solvent system that separates the different polar lipids, while the neutral lipids migrate at the solvent front[41]. Lipids bands were visualized with primuline (0.01% in 80% acetone) under UV light, and scraped off. Fatty acids methyl esters (FAME) were prepared by trans-methylation of fatty acids with methanol:sulfuric acid (97.5:2.5, v/v). Fatty acids quantitative analysis was performed using gas chromatography (430 Gas Chromatograph, Varian) at 210ºC, equipped with hydrogen flame ionization detector, heptadecanoic acid (C17:0) as an internal standard. The double bond index (DBI) was calculated as in Equation 1.

$$\mathrm{DBI} = \frac{(\%\text{monodienoic acids}) + 2(\%\text{dienoic acids}) + 3(\%\text{trienoic acids})}{100}$$

Equation 1 – Calculation of double bound index

3.9. Photosynthetic pigments extraction and quantification

Photosynthetic pigments were extracted from inoculated and mock inoculated ground leaves by adding 1.5 mL of methanol to 20 mg of plant material, and incubated in the dark at 4ºC for 48 hours. Samples were centrifuged at 1200 *g* for 5 minutes and the supernatant was collected. The absorbency was measured at 470, 652.4 and 665.2 nm and the pigment's concentration for chlorophyll A (Chla), chlorophyll B (Chlb) and total carotenoids was calculated as previously described[42].

3.10. Sugar extraction and quantification

Samples (0.1 - 0.2 mg fresh weight) were dried for 48 hours at 70ºC and weighted to calculate the water content and dry weight (DW). To each sample ethanol 80% (v/v) was added (1/10, g

DW/v) and homogenized for 5 minutes. Samples were heated to 80ºC for 30 minutes and centrifuged at 16000g for 15min, based on Guy et al., 1992[43]. Supernatant was collected, dried overnight at 70ºC and used to measure soluble and sugars. Pellet was collected and dried overnight at 70ºC and used to measure starch (insoluble sugars). Sucrose concentration was measured by adding 0.25 mL of resorcinol (1%) and 0.75 mL of HCL (30%) to 0.1 mL of each sample. Samples were kept at 100ºC for 10 minutes. Reducing sugars concentration was determined by adding 1mL of Dinitrosalicylic Acid (DNS) (0.25g DNS + NaOH 2 M) to 0.1 mL of each sample. Samples were kept at 80ºC for 8 minutes. Absorbance was measured at 470 and 520 nm for sucrose and reducing sugars, respectively[44]. The dried pellet was submitted to acid hydrolysis, as previous described[45], samples were centrifuged for 10 minutes at 15000 *g* and supernatant collected. Measurements of released D-Glucose were performed as described above for reducing sugars.

3.11. Determination of H_2O_2 content

H_2O_2 content was determined, as described in Childs & Bardsley, 1975[46] based on the oxidation the chromogen 2′,2-azino-di(3-ethyl-benzathiazoline-6-sulphonic acid) catalyzed by a peroxidase in the presence of H_2O_2. Briefly, 100 mg of plant material were homogenized in a phosphate buffered saline solution (PBS) with 1-4% (w/v) of insoluble polyvinylpolypyrrolidone ($PVPP_{40000}$). Samples were centrifuged at 16000 *g* for 1 min and the supernatant was collected and used for the assay. Concentration of hydrogen peroxide was measured spectrophotometrically at 405 nm using a standard curve with known concentrations of H_2O_2. Three biological replicates and two technical replicates were used

3.12. Antioxidant capacity assay

Total antioxidant capacity was measured spectrophotometrically at 405 nm using the antioxidant assay kit (Sigma-Aldrich) according to manufacturer's instructions. A standard curve with known concentrations of Trolox (Sigma-Aldrich) was used and data were normalized by protein content. Three biological replicates and two technical replicates were used.

3.13. Lipid peroxidation

For lipid peroxidation analysis, the thiobarbituric acid (TBA) reacting substance was used as described in Hodges et al., 1999[47]. Briefly, 100 mg of frozen samples were homogenized in

ethanol 80% (v/v) and centrifuged at 14000 g for 5 minutes at 4°C. The supernatants reacted with TBA solution at 95 °C for 30 minutes. Absorbance at 440, 532 and 600 nm was determined after a 10 minutes centrifugation at 14000 g, 4°C. Malonaldehyde (MDA) is considered an index of general lipid peroxidation and its concentration was calculated as described in Equation 2.

$$\text{MDA(nmol.ml}^{-1)} = \frac{[(\text{A-B}) \times 106]}{157000};$$

$$\text{A}=[(Abs_{532}+\text{TBA})- (Abs_{600}+\text{TBA})]-[(Abs_{532}-\text{TBA})-(Abs_{600}-\text{TBA})];$$

$$\text{B}= [(Abs_{440}+\text{TBA})- (Abs_{600}+\text{TBA})] \times 0{,}0571$$

Equation 2 – Quantification of MDA

4. Results

4.1. *P. viticola* inoculated grapevine and control samples present distinct metabolic profiles

The modulation of *V. vinifera* cv Trincadeira metabolome in response to *P. viticola* inoculation (Figure 2) at 6, 12 and 24hpi were characterized by direct infusion FTICR-MS. The methanol fraction of the leaf metabolome was analysed by direct infusion FTICR-MS in both ionization modes. The ion peak list for each timepoint and ionization mode was aligned by an in-house developed Python-based script and masses were submitted to the MassTRIX server for metabolite identification. From the initial total of 11406 ion peaks detected in both ESI(+) and ESI(-) a total of 1460 metabolites belonging to various chemical groups were putatively or tentatively identified (Table 2, Appendix 2). A data matrix considering only the masses putatively assigned to a metabolite was submitted to MetaboAnalyst 3.0 for statistical analysis.

Application of the multivariate analysis PLS-DA revealed a separation between inoculated and control samples at all of the studied time-points and ESI modes (Figure 3) indicating distinctive responses to pathogen attack. A total of 40 metabolites presenting significant modulation ($p \leq 0.05$) between inoculated and control samples at each time-point were identified (Table 2).

Table 2 - Number of peaks, identified masses and differently accumulated metabolic entities identified with ESI(+) and ESI(-) after inoculation.

		Peaks		Identified masses		Differently accumulated	
	Ionization Mode	**ESI(+)-MS**	**ESI(-)-MS**	**ESI(+)-MS**	**ESI(-)-MS**	**ESI(+)-MS**	**ESI(-)-MS**
Time Points	6hpi	2512	1318	264	145	4	5
	12hpi	1365	1331	247	160	10	8
	24hpi	3726	1154	520	124	7	6
	Total	11406		1460		40	

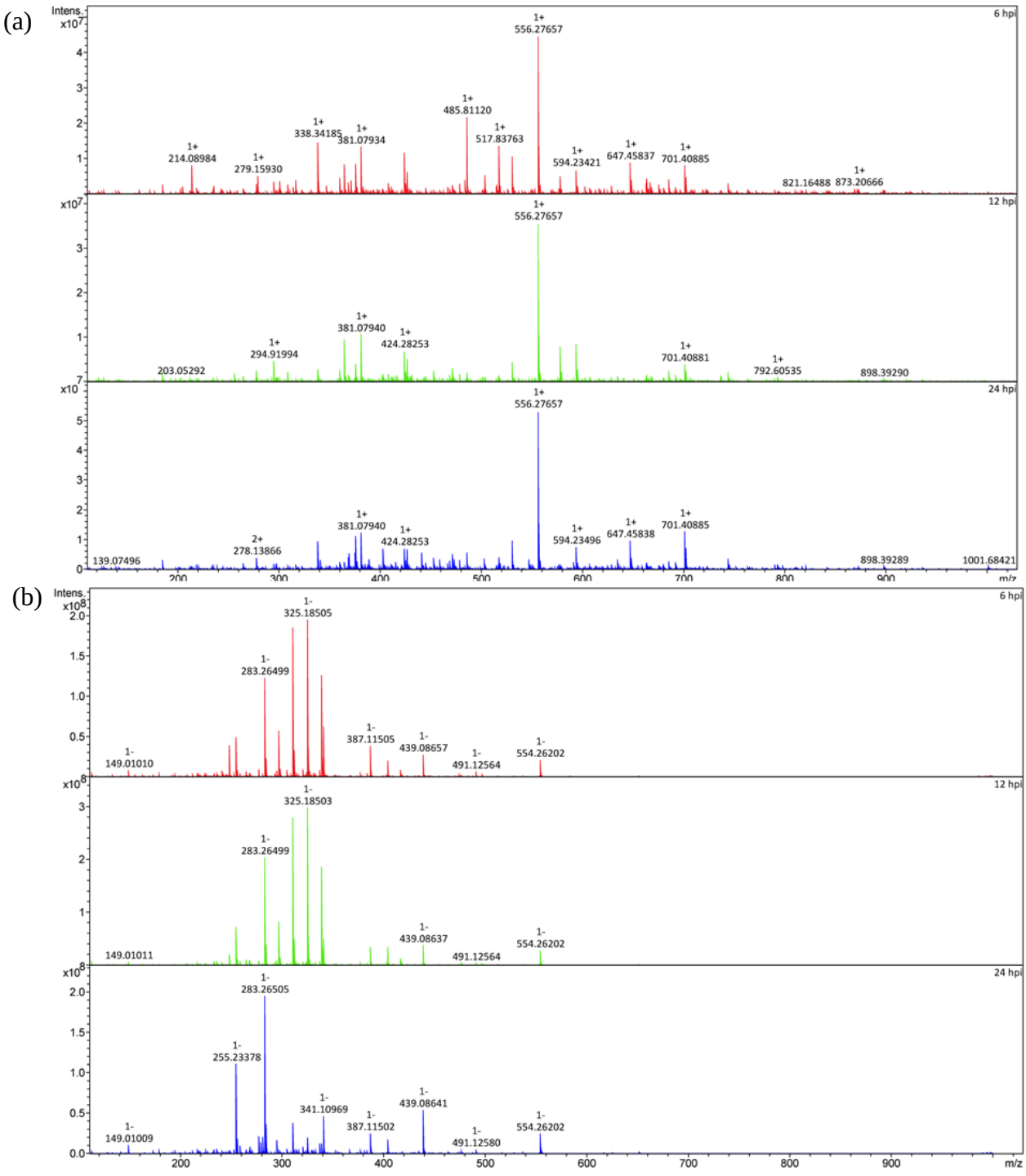

Figure 2 - Cumulative mass spectra of *Vitis vinifera* cv Trincadeira – *P. viticola* at 6, 12 and 24 hpi.

Data were acquired in (a) positive (ESI+) and (b) negative (ESI−) electrospray modes performing direct infusion analysis in the range 100-1100 m/z. The software DataAnalysis 4.1 was used for the creation of mass spectra.

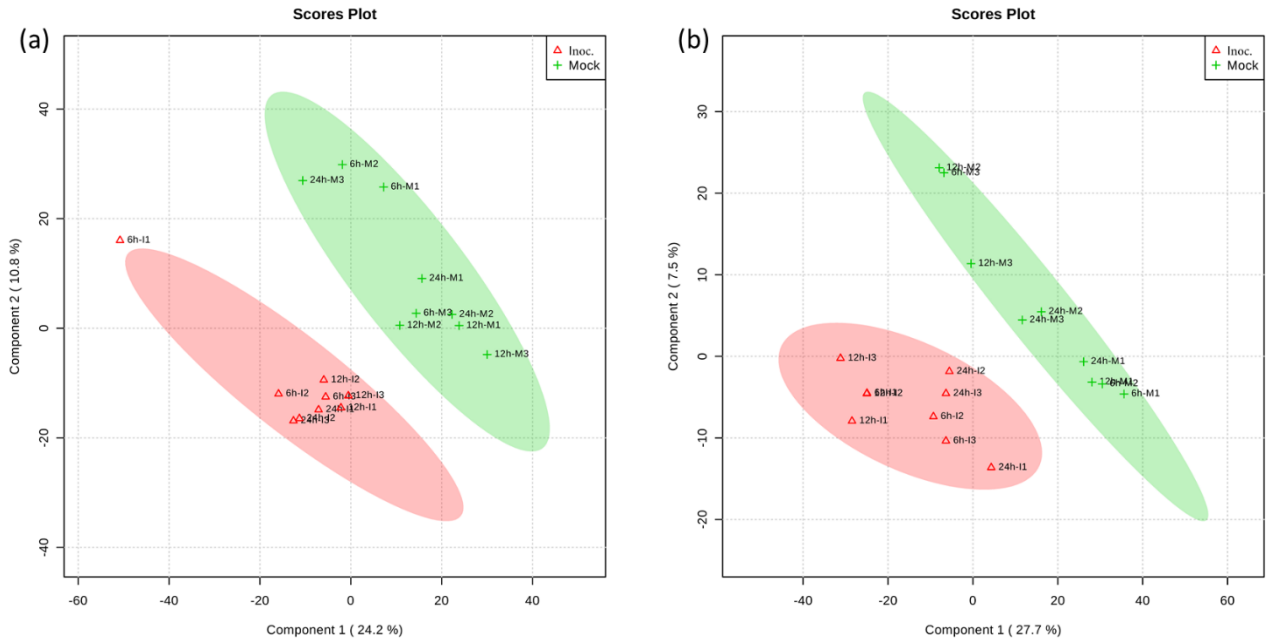

Figure 3 - Partial least squares-discriminant analyses (PLS-DA) PC1/PC2 score plots of identified secondary metabolite profiles of *Vitis vinifera* cv. Trincadeira at 6, 12 and 24 hours after inoculation with *P. viticola*.

(a) (ESI +); (b) (ESI -); In the score plots, the ellipse represents the Hotelling T2 with 95% confidence interval. Three (3) biological replications were performed per treatment.

Differentially accumulated metabolites were putatively annotated in functional categories using an in-house build python program (unpublished data) which performs database search (KEGG, Lipid Maps and KnapSACK) for a possible functional classification (Appendix 1). After *P. viticola* inoculation, lipids were the most altered class at the three inoculation time-points representing 78% of the differentially accumulated metabolites at 6hpi, 39% at 12hpi and 54% at 24hpi (Figure 4). Carbohydrates were the second most altered class at both 6 and 12hpi, being mainly down accumulated (Figure 4). At 12 and 24hpi the alkaloid class was also modulated by *P. viticola* inoculation.

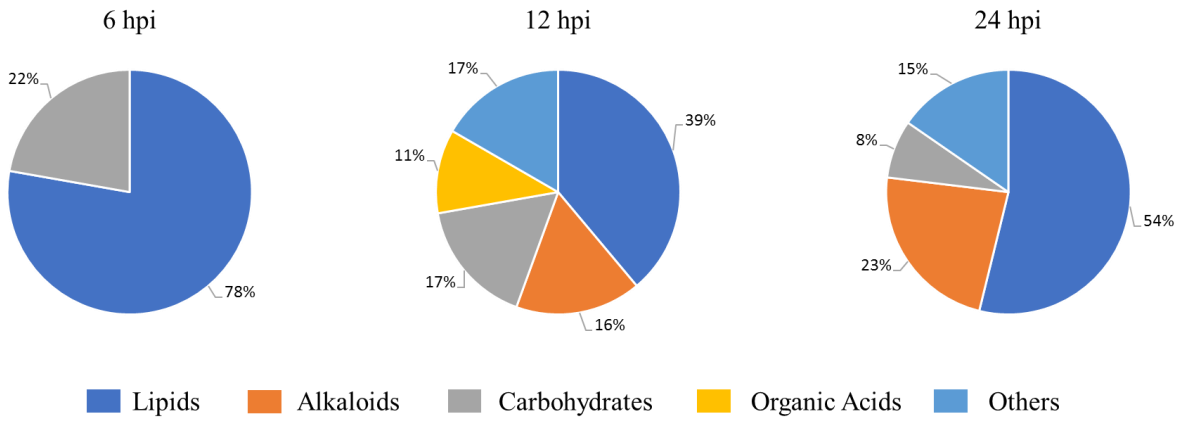

Figure 4 - Differently accumulated metabolites major classes in infected leaves. Putative major class for each different accumulated metabolite are represented for the 3 time point (6, 12 and 24 hpi).

4.2. *P. viticola* modulates lipid and fatty acid content indicating their involvement in pathogenesis

Upon *P. viticola* challenge, the relative content of infected *Vitis vinifera* cv Trincadeira leaves in lipids and fatty acids (FAs) was considerably altered (Figure 4, Figure 5).

Among the lipids identified by direct infusion FTICR-MS that were modulated by the pathogen, flavonoids class were the most altered (Figure 5). All of the identified flavonoids were down-accumulated after *P. viticola* inoculation, with exception of the m/z 425.13633 (ESI+) assigned to several flavonoids with identical monoisotopic masses. One of the putative assignments may be Ulexone B.

The second most altered lipid class was fatty acids and conjugates, also down-accumulated in the inoculated samples, where the fatty acid Lipoic acid (m/z 205.03623) is an example (Figure 5).

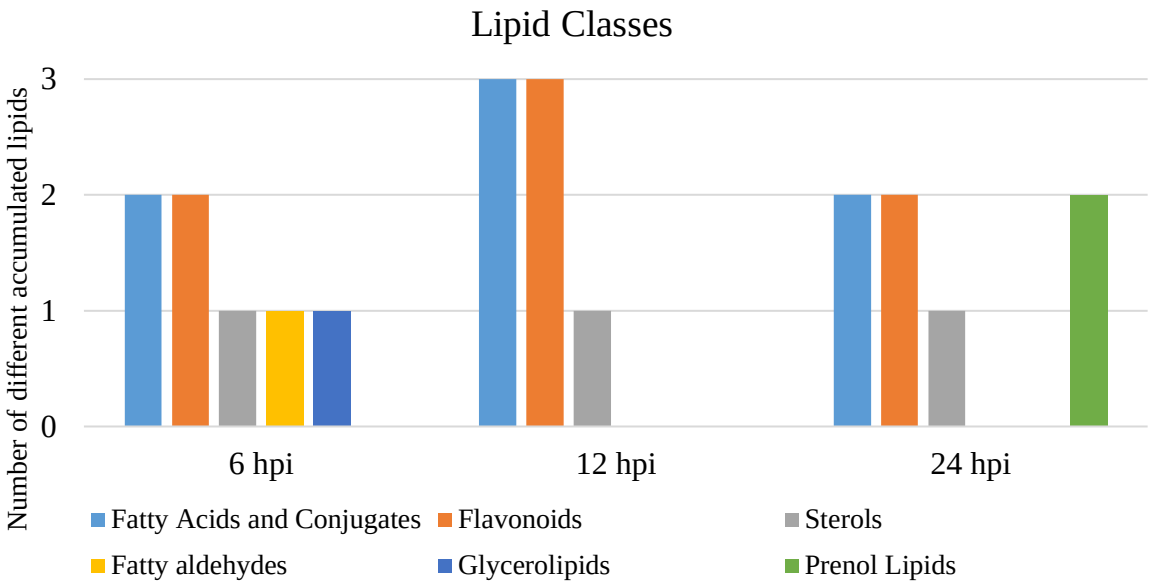

Figure 5 - Secondary classes of differently accumulated lipids at 6, 12 and 24 hpi.

Putative secondary class for each different accumulated lipid metabolite for the 3 time points.

By Gas Chromatography we were able to identify the most common FAs, such as hexadecenoic acid (C16:0), linoleic (C18:2), and linolenic acids (C18:3), highly abundant in Trincadeira leaves and trans-hexadecaenoic acid (C16:1t), stearic (C18:0) and oleic acids (C18:1) less abundant (Table 3).

Table 3 – Gas Chromatography measurements of total fatty acid percentage at 6, 12 and 24 hpi.

* Represents the statistically different between inoculated and control samples ($p<0.05$)

		C16:0	C16:1t	C18:0	C18:1	C18:2	C18:3	C18:3/C18:2
6 hpi	**Control**	16 ± 0.8	3 ± 0.1	1.8 ± 0.5	3.2 ± 0.4	13.7 ± 0.5	62.3 ± 2.1	4.6 ± 0.3
	Inoculated	16.8 ± 0.3	2.9 ± 0.2	1.9 ± 0.5	**3.7* ± 0.2**	14.1 ± 0.7	60.6 ± 1.1	4.3 ± 0.3
12 hpi	**Control**	17.0 ± 1.2	3.1 ± 0.3	2.1 ± 0.5	3.2 ± 0.4	14.0 ± 0.8	60.7 ± 1.0	4.4 ± 0.2
	Inoculated	16.7 ± 0.7	3.1 ± 0.1	1.9 ± 0.2	3.2 ± 0.1	14.8 ± 0.3	60.4 ± 0.9	**4.1* ± 0.1**
24 hpi	**Control**	16.8 ± 0.8	2.9 ± 0.3	1.6 ± 0.3	3.6 ± 0.2	15 ± 0.4	60.1 ± 0.5	4.1 ± 0.1
	Inoculated	17.7 ± 0.2	3 ± 0.1	1. ± 0.1	**3.9* ± 0.1**	15.1 ± 0.2	**58.8* ± 0.2**	**3.9* ± 0.1**

After *P. viticola* inoculation, oleic (C18:1) and linolenic (C18:3) acids were the most affected exhibiting an increase of 14.5% at 6hpi and 15.4% at 24hpi (C18:1) and a decrease of ~2.3% at 24 hpi (C18:3) (Table 3). This decrease in C18:3 content also relates to the decrease on the C18:3/C18:2 ratio at 12h hpi (Table 3).

We were also able to identify several polar lipids, such as phosphatidylcholine (PC), phosphatidylethanolamine (PE), Mono and Di – galactosyldiacylglycerols (MGDG and DGDG), phosphatidilglycerol (PG), phosphatidic acid (PA), phosphatidylinositol (PI) as well as neutral lipids such as triacylglycerol (TAG), free fatty acids (FFA). The major lipids identified were the plastidial lipids, MGDG and DGDG, followed by extraplastidial lipids, PC and PE. In lower amounts are the storage lipids (triacylglycerol, TAG), signaling lipids (PA and PI) and the free FA, that can also act as signaling lipids (Table 4). Although no significant differences were observed in the proportions of each lipid class, between inoculated and control samples, a tendency for a decrease in MGDG content accompanied by an increase in free FAs was observed (Table 4). Also, some differences were found in the fatty acid composition of MGDG, neutral lipids and PA. A reduction of the 18:3/18:2 was observed for MGDG (~3 %) and PC (~6 %), whereas increases in the saturated C16:0 (~12.2%) and C18:0 (~53.3%) and the monounsaturated C18:1(~19.7%) were recorded for TAG, FFA and "others", respectively (Table 4).

Table 4 – Fatty acid percentage at 6 hpi, measured by thin layer chromatography.

C and I represents, respectably, control and inoculated samples, *Represents statistically significant differences between the inoculated and control replicates ($p \leq 0.05$; Mann-Whitney U test).

		C16:0	C16:1t	C18:0	C18:1	C18:2	C18:3	µgFA/gFW	DBI	C18:3/18:2
MGDG	C	2,25 ± 0,11	0	0,45 ± 0,14	0,70 ± 0,18	3,61 ± 0,02	92,99 ± 0,19	1121,37 ± 42,48	2,87 ± 0,00	25,79 ± 0,08
	I	2,22 ± 0,41	0	0,37 ± 0,03	1,12 ± 0,24	3,7 ± 0,07	92,69 ± 0,47	967,49 ± 85,97	2,87 ± 0,01	**25,04* ± 0,32**
DGDG	C	20,38 ± 4,24	0	2,11 ± 0,68	1,06 ± 0,16	3 ± 0,37	73,46 ± 5,44	548,4 ± 116,48	2,27 ± 0,15	25,42 ± 4,94
	I	20,52 ± 0,98	0	1,64 ± 0,06	1,02 ± 0,05	2,51 ± 0,08	74,31 ± 0,78	511,75 ± 7,53	2,29 ± 0,03	29,63 ± 0,65
PC	C	36,10 ± 1,94	0	5,06 ± 1	6,53 ± 0,48	33,51 ± 2,00	18,81 ± 1,42	242,84 ± 24,16	1,30 ± 0,08	0,56 ± 0,001
	I	36,39 ± 4,73	0	4,97 ± 0,80	7,35 ± 0,48	33,58 ± 3,20	17,71 ± 1,84	240,53 ± 29,93	1,28 ± 0,12	**0,53* ± 0,00**
PE	C	42,91 ± 6,18	0	3,72 ± 1,29	1,16 ± 1,64	40,73 ± 3,83	12,64 ± 2,18	151,76 ± 16,96	1,19 ± 0,16	0,31 ± 0,03
	I	40,25 ± 3,30	0	2,92 ± 0,01	2,15 ± 0,19	41,79 ± 2,56	12,88 ± 0,94	160,478 ± 9,48	1,24 ± 0,08	0,301 ± 0,00
TAG	C	14,38 ± 0,11	0	4,82 ± 0,33	4,39 ± 0,24	42,40 ± 0,11	34,01 ± 0,31	125,06 ± 5.82	1,91 ± 0,01	0,80 ± 0,01
	I	13,68 ± 0,80	0	4,34 ± 0,62	**5,25* ± 0,55**	41,26 ± 0,80	34,26 ± 0,64	122,15 ± 11,74	1,90 ± 0,03	0,81 ± 0,01
PG	C	34,74 ± 5,26	34,45 ± 2,45	3,82 ± 0,65	13,83 ± 2,46	4,12 ± 0,83	8,32 ± 2,92	68,68 ± 10,93	0,44 ± 0,12	2,02 ± 0,32
	I	37,64 ± 6,54	30,67 ± 3,47	3,45 ± 1,91	16,75 ± 2,76	4,25 ± 2,45	8,19 ± 2,61	59,75 ± 11,39	0,41 ± 0,12	1,74 ± 0,36
Cuticle	C	32,07 ± 4,25	0	19,77 ± 4,17	12,79 ± 3,34	25 ± 4,16	16,49 ± 3,97	34,63 ± 4,06	1,08 ± 0,19	0,62 ± 0,08
	I	40,29 ± 5	0	**30,31* ± 3,17**	9,96 ± 1,89	14,52 ± 3,96	7,73 ± 6,28	37,23 ± 1,75	0,55 ± 0,23	0,72 ± 0,02
PA	C	28,93 ± 13,26	0	13,94 ± 18,19	0	47,34 ± 25,33	7,91 ± 11,19	12,46 ± 2,51	1,17 ± 0,70	0,25 ± 0,25
	I	24,22 ± 21,80	0	13,71 ± 6,01	4,65 ± 4,890	31,87 ± 16,24	17,08 ± 8,89	16,79 ± 5,10	1,36 ± 0,60	0,35 ± 0,26
PI	C	34,42 ± 3,07	0	11,04 ± 7	3,76 ± 3,44	19,62 ± 3,07	27,38 ± 2,49	24,76 ± 4,90	1,27 ± 0,10	1,57 ± 0,28
	I	33,65 ± 3,94	0	14,81 ± 6,01	4,32 ± 1,82	18,68 ± 1,87	25,38 ± 4,23	22,53 ± 5,61	1,11 ± 0,12	1,56 ± 0,27
Free FA	C	32,06 ± 1,43	0	55,85 ± 3,79	6,69 ± 0,76	3,86 ± 1,35	2,94 ± 2,66	48,38 ± 16,90	0,22 ± 0,11	0,76 ± 0,44
	I	**35,96* ± 1,27**	0	54,45 ± 0,23	4,53 ± 0,40	3,00 ± 0,60	2,06 ± 0,98	57,8 ± 19,51	0,17 ± 0,03	0,50 ± 0,29

4.3. Oxidative stress, lipid peroxidation and modulation after *P. viticola* inoculation

The production of Reactive Oxygen Species (ROS) as signaling molecules in plants is one of the earliest cellular response to pathogen recognition, commonly described as oxidative burst. Higher ROS content has the capacity to fragment the fatty acids within the membranes into structurally diverse products that are known in humans to be specifically sensed by the organism and used to direct downstream responses[48]. Our data shows an increase of ROS in inoculated samples compared to controls. Lipid peroxidation is increased among all time points, especially at 6 hpi and at 24 hpi. Despite ROS and lipid peroxidation increase in inoculated samples, antioxidant capacity was not altered significantly (Figure 6).

(a)

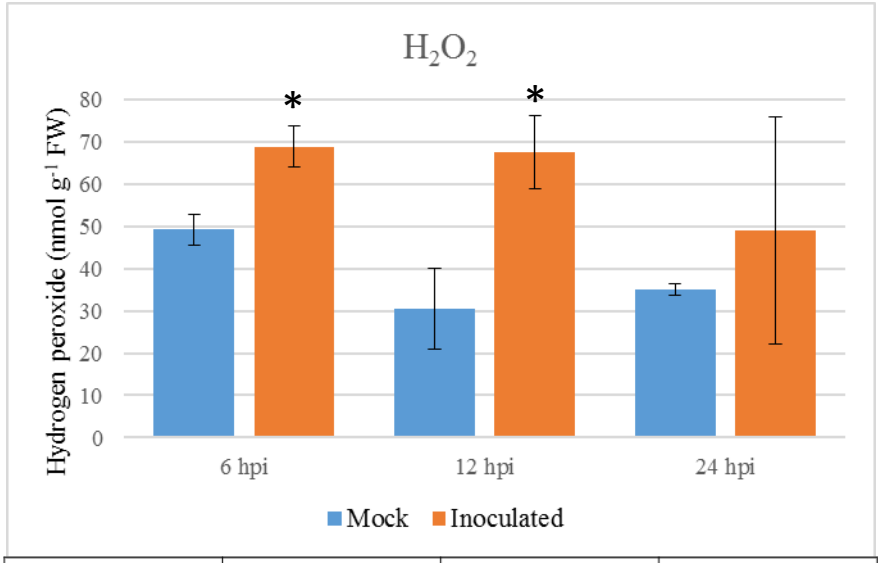

	6 hpi	12 hpi	24 hpi
Mock	49.266 ± 3.682	30.544 ± 9.46	35.055 ± 1.414
Inoculated	68.937 ± 4.481	67.609 ± 8.522	49.163 ± 26.879

(b)

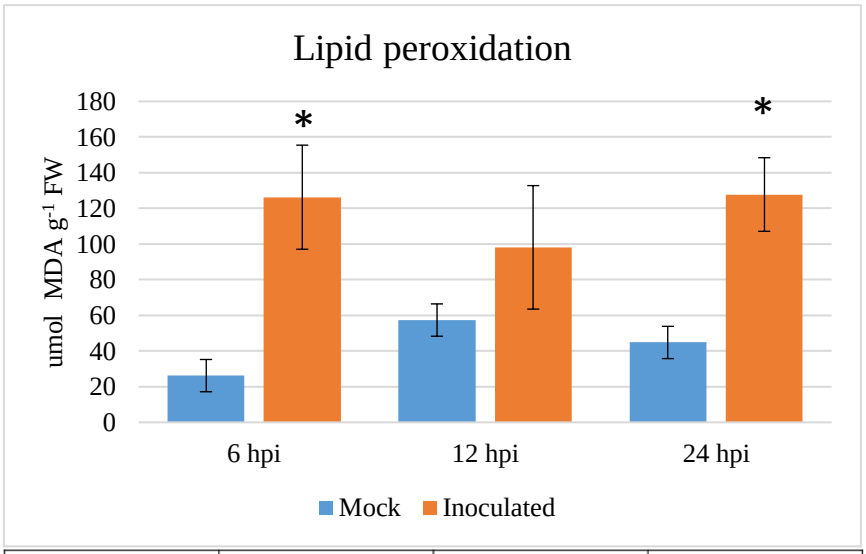

	6 hpi	12 hpi	24 hpi
Mock	26.216 ± 2.055	57.369 ± 6.832	44.803 ± 13.773
Inoculated	126.284 ± 29.191	98.159 ± 34.623	127.789 ± 20.651

(c)

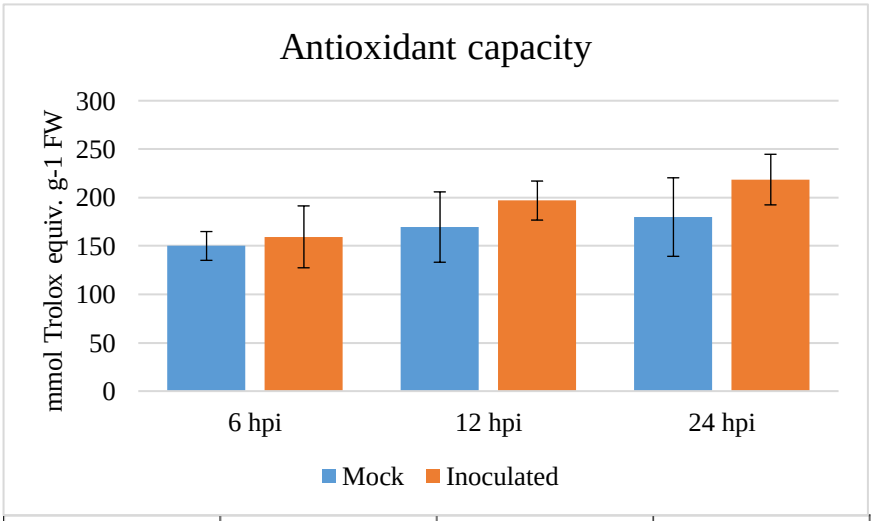

	6 hpi	12 hpi	24 hpi
Mock	149.975 ± 14.854	169.464 ± 36.309	179.810 ± 40.558
Inoculated	159.333 ± 31.953	196.885 ± 20.165	218.520 ± 26.142

Figure 6 - ROS production, antioxidant capacity and lipid peroxidation in *V. vinifera* cv Trincadeira inoculated leaves with *P. viticola* at 6, 12 and 24 hpi.

(a) Hydrogen peroxide (µmol Hydrogen peroxide g^{-1} FW); (b) MDA content (nmol MDA equiv. g^{-1} FW); (c) total antioxidant capacity (µmol Trolox equiv. mg^{-1} protein). *represents statistically significant differences between the inoculated and control replicates ($p \leq 0.05$; Mann-Whitney U test).

4.4. Changes in the content of carbohydrates after *P. viticola* inoculation is indicative of a general remobilization of sugars

The photosynthesis process allows the conversion of carbon dioxide into sugars which are unsurprisingly detected in the leaf extracts. A limitation performing direct infusion FTICR-MS analysis is the inability to distinguish between various common metabolites with identical monoisotopic masses, such as several carbohydrates (Appendix 2). The majority of the identified carbohydrates by direct infusion FTICR-MS are down-accumulated, with exception of the m/z 543.13206 putatively assigned to the Raffinose family of oligosaccharides (RFOs), glucose or glucose derivatives.

We have further conducted glucose, fructose, sucrose and starch quantification as well as the quantification of major pigments (Chla, Chlb and carotenoids) as photosynthesis biomarkers.

Photosynthetic pigments showed no significant variation in the first 24h of infection suggesting no variation in photosynthesis rate (Figure 7). Reducing sugars in inoculated samples have a 2-fold increase at 6 hpi (mock inoculated: 109.24 ± 9.55 mg g^{-1} DW; inoculated: 212.45 ± 43.98 mg g^{-1} DW). At 12hpi an increase in starch concentration was observed in inoculated samples (mock inoculated: 99.44 ± 3.38 mg g^{-1} DW; Inoculated: 144.52 ± 0.38 mg g^{-1} DW) (Table 5).

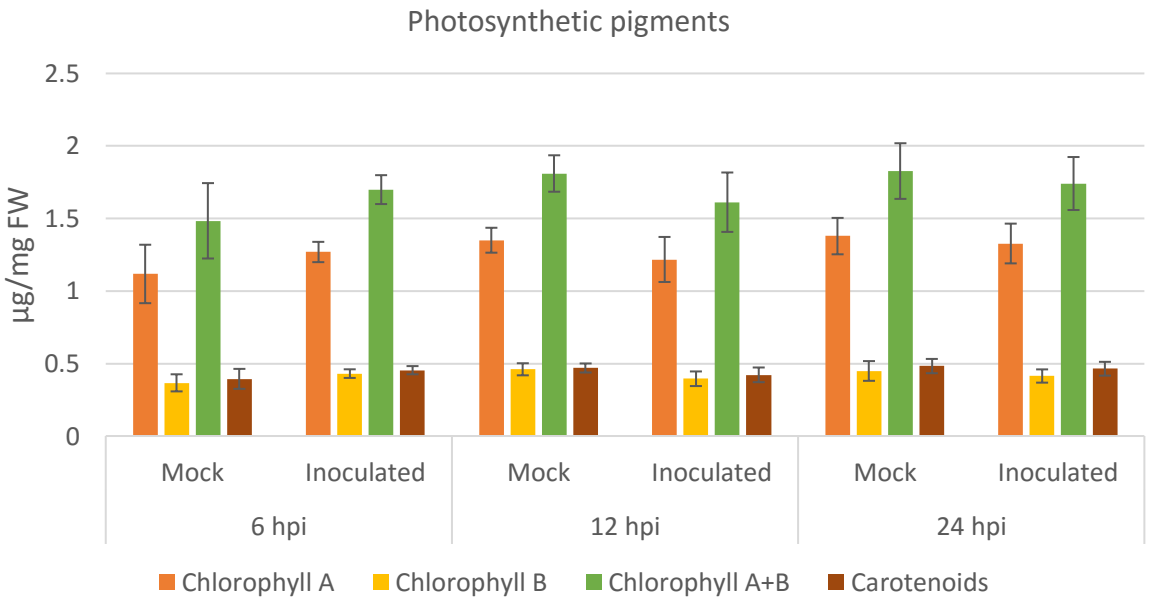

Figure 7 - Chlorophyll A, B and Carotenoids concentration in mock and inoculated leaves. Photosynthetic pigments quantification in mock and infected leaves at 6, 12 and 24 hpi. Results in µg mg^{-1} FW.

Table 5 - Reducing sugars, sucrose and starch quantification in control and inoculates. Results in mg sugar g^{-1} DW. *Statistically significant differences between the inoculated and control replicates ($p \leq 0.05$; Mann-Whitney U test).

		6 hpi	12 hpi	24 hpi
Reducing Sugars	Control	109.24 ± 9.55	159.81 ± 2.53	112.57 ± 8.66
	Inoculated	212.45 ± 43.98*	143.09 ± 22.43	131.92 ± 27.91
Sucrose	Control	50.42 ± 4.69	39.64 ± 4.25	26.60 ± 7.61
	Inoculated	44.74 ±5.99	38.59 ± 6.30	38.49 ± 5.76
Total Soluble Sugars (TSS)	Control	159.66 ± 13.81	199.45 ± 6.78	139.17 ± 5.12
	Inoculated	257.19 ± 49.66*	181.68 ± 28.14	170.40 ± 31.72
Starch	Control	87.59 ± 1.93	99.44 ± 3.38	119.33 ± 5.68
	Inoculated	93.08 ± 7.09	144.52 ± 0.38*	115.37 ± 21.12
Total Sugars (TS)	Control	247.26 ± 13.47	298.89 ± 10.16	258.50 ± 6.59
	Inoculated	350.26 ± 55.93	326.20 ± 27.77	285.78 ± 27.81

4.5. Modulation of alkaloid metabolites after *P. viticola* inoculation

Alkaloids are a very diverse group of natural products, appearing in many organism especially within plants, where they have the greatest variability of structure and functions[49,50].

Our data shows a general decrease in alkaloids at 12 hpi (Figure 4). At 24 hpi two alkaloids were found to be more accumulated in the *V. vinifera* cv Trincadeira inoculated samples, at the m/z 617.25396 (ESI-) putatively assigned to the corresponding $[M+Cl35]^-$ ion of Aralionine A and m/z 347.11690 (ESI-) putatively assigned to several alkaloids chairing the same monoisotopic mass (Appendix 2).

4.6. Pathway analysis and expression analysis

From our results, we have selected genes related to lipid metabolism to access the expression of key enzymes of their biosynthetic pathways. For the biosynthesis of lipoic acid, the coding gene *Lipoyl Synthase* was selected. For flavonoids biosynthesis the coding genes for the enzymes flavonol synthase/flavanone 3-hydroxylase, dihydroflavonol reductase and flavonoid-3,5'-hydroxylase were analyzed (Figure 8). Also, based on other studies[13,51] we have selected the genes related to the biosynthesis of catechin (*ANR*), epicatechin (*Lar2*) and saturated fatty-acids C16:0 and C18:0 (*FatB*).

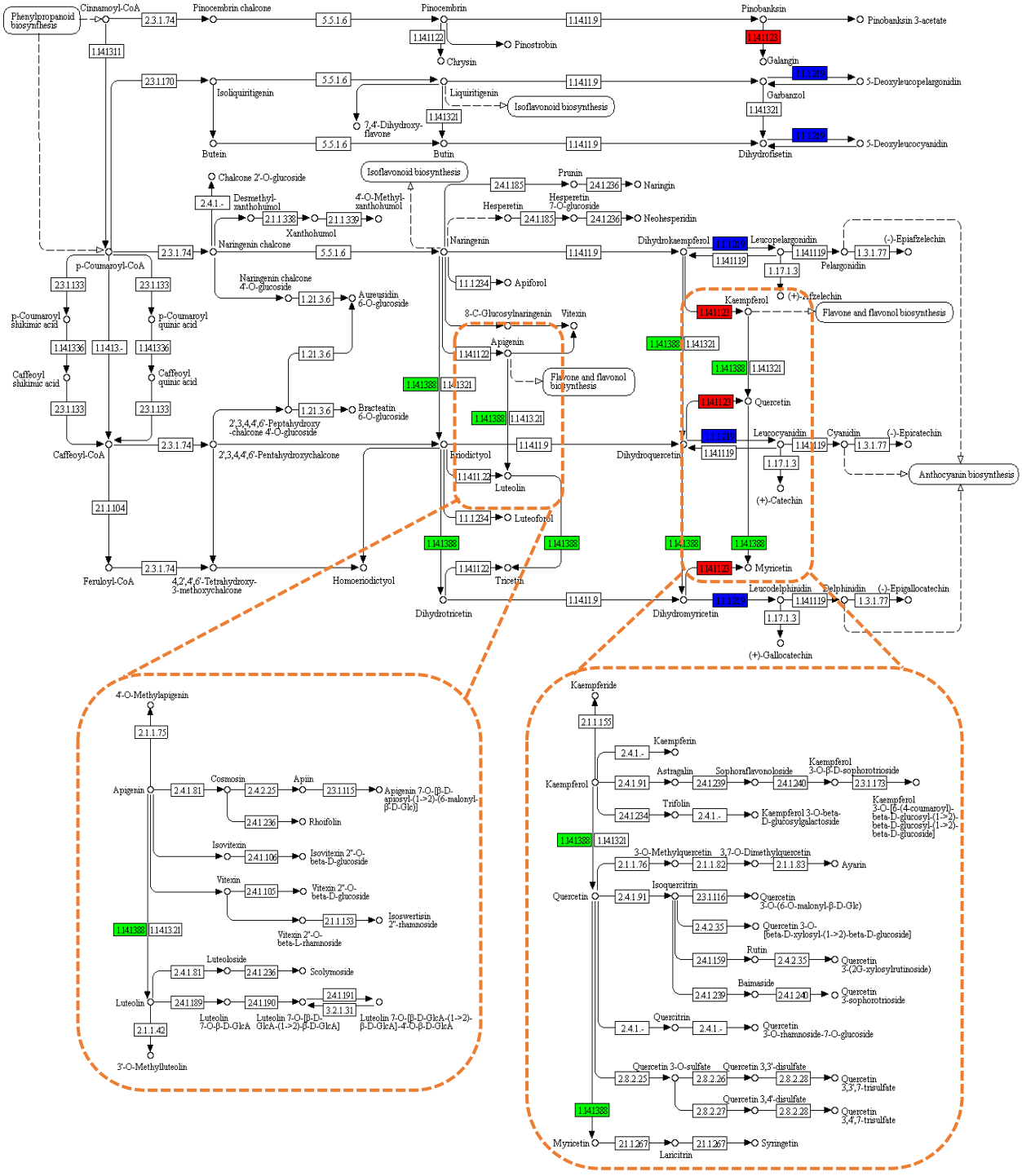

Figure 8 – Flavonoid biosynthesis pathway.

Highlighted in orange is the Favone and Flavonol biosynthesis pathway. Marked in red is the *FLS* gene, in green the *F3'5'H* gene and in blue *DFR* gene. Images adapted from KEGG.

Both *ARN* and *FatB*, showed the same trend, being up-regulated only at 24hpi, while *LAR2* presented an expression increase at 6hpi. *Lip A* for lipoic acid biosynthesis remained unaltered suggesting that the decrease in lipoic acid accumulation after inoculation may be related to lipid alterations due to lipid peroxidation. *Flavonol Synthase/Flavanone 3-hydroxylase* comprises several genes, in grapevine 7 genes are described, two of them splicing variants. We have analysed the expression of 6 *FLS* genes and only *FLS-F* presents an expression increase after inoculation, the majority of the genes were strongly down-regulated (*FLS-A*: -3.4 ± 0.99 to -14.6 ± 2.4 fold-change; *FLS-D*: -6.4 ± 4, -20.1 ± 1.8 fold-change; *FLS-E*: 1.36 ± 0.1 to -2.7 ± 0.5 fold change). *Flavonoid-3,5'-hydroxylase* presented the same expression trend as *LAR2* and *FatB*, while *Dihydroflavonol reductase* was down-regulated at 6hpi (Figure 9).

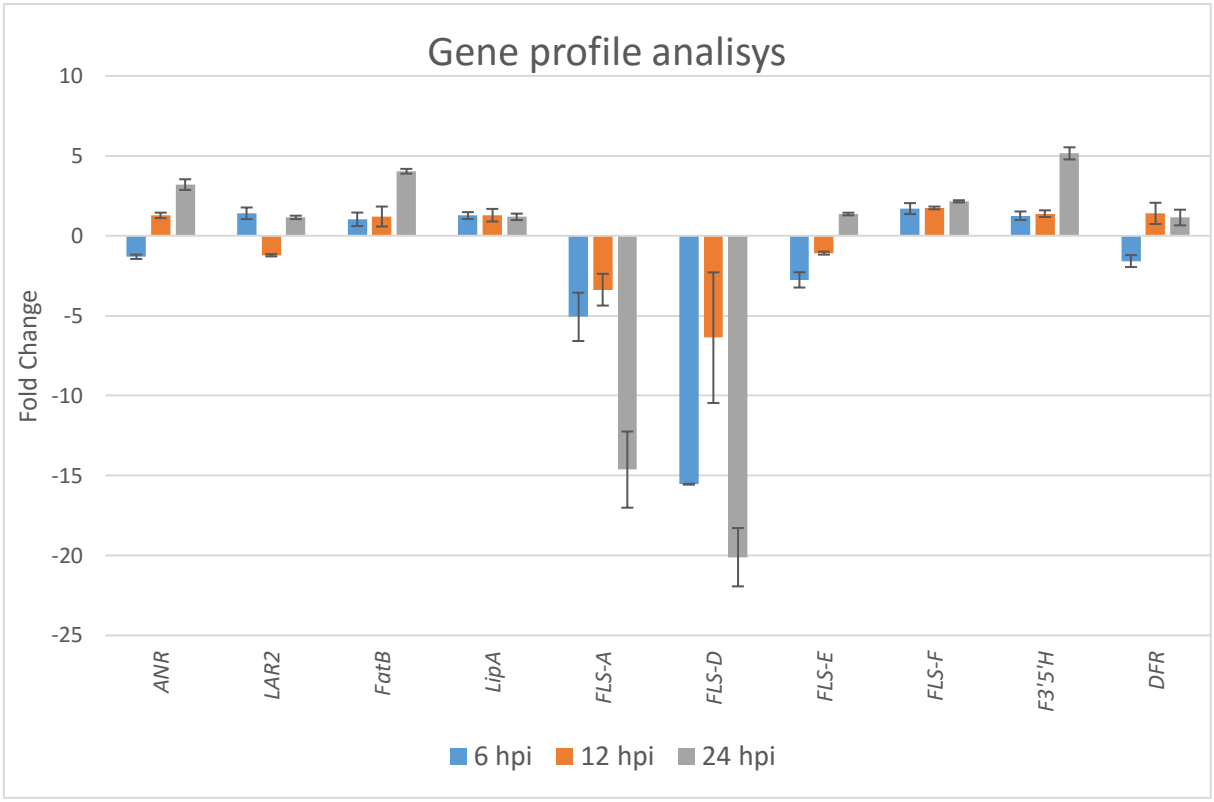

Figure 9 - Gene expression profile in inoculated leaves.

For each time point (6, 12 and 24 hpi) gene transcripts fold-change relative to controls are represented for *ANR, LAR2, FatB, LipA, FLS-A*, FLS-*D, FLS-E, FLS-F, F3'5'H* and *DFR*. Fold-change values are relative to expression in mock leaves.

5. Discussion

In the present work, we analyzed the compatible interaction between *Vitis vinifera* cv. Trincadeira and *Plasmopara viticola*. Previous studies have been conducted in this compatible interaction [52–56], but very few analyzed the first hours of infection [13,22,57].

5.1. Lipid metabolism is affected by *P. viticola* in the first hours of inoculation

Lipids are a diverse group of compounds with a variety of biological roles, including a structural role, signalling molecules, protection against biotic and abiotic stresses and energy storage[58,59].In the present work, over half of the significant accumulated masses were putatively annotated as lipids (Figure 4 and Appendix 2), being most of them putatively classified as flavonoids or fatty acyls. The accumulation of phenylpropanoids and flavonoids upon pathogen infections is extensively documented in multiple plant biological models, being mostly associated to the establishment of an incompatible interaction[13,55]. Flavonoids were also known to decrease the pathogen development and severity in susceptible cultivars[52,60]. Our results show a decrease in flavonoid accumulation, with exception of m/z 425.13633 (ESI+) (assigned to several flavonoid metabolites sharing the same monoisotopic mass). This flavonoid is accumulated in the inoculated samples in all of the analyzed time-points. A possible annotation for this ion is Ulexone B (Appendix 2), previously reported as more accumulated in wheat upon *Fusarium Graminearum* infection[61].

We have further analyzed the transcript profiles *FLS* coding gens. Our results show reduction in transcript abundance of the majority of *FLS* coding genes in infected leaves. However, one *FLS* transcript (*FLS-F*: 1.7 ± 0.34, 1.7 ± 0.08, 2.1 ± 0.06 fold-change at 6, 12 and 24 hpi respectively) is over-expressed, thus it may be associated to the synthesis of the flavonol that appear more accumulated in the inoculated samples (m/z 425.13633 (ESI+)). A possible protective role as been attributed to flavonoids in susceptible cultivars, it suggested that constitutive flavonoids are able to slow down the infection, and higher amounts of flavonoids decrease the susceptibility of grapevines to downy mildew [52,60]. The lower accumulation of flavonoids encountered in infected leaves, and the general down-regulation of FLS coding genes, may suggest a suppression of resistances and/or defense response endogenous to flavonoids caused by *P. viticola*.

Among the saturated FA found in plant lipids, Hexadecanoic (C16:0) and Stearic acid (C18:0) are the most common. Saturated fatty acids are involved in the permeability control of cell lipid

membrane, in which, an increase content contributes to a more impermeable cell membrane [11,62]. Furthermore, hexadecanoic acid has been marked as possible marker for resistance against *Plasmopara viticola* [11]. The expression profile of *FatB* suggest an increase in saturated fatty only at 24hpi (4.0 ± 0.15 fold-change), despite a slight increase in C16:0 at 24hpi, no significant differences are observed in total saturated fatty acids (Table 3).

Regarding the composition of the major membrane FA, our results demonstrate an increase in C18:1 at 6 and 24hpi (Table 3). Although this FA was associated to plant defense, by stimulation or binding to proteins that can promote anti-cell-death[63,64] and to azelaic acid (AZA) biosynthesis, contributing for the establishment of systemic acquired resistance (SAR), no AZA was detected in our study, thus we hypothesize that SAR is not established on this interaction

Previous works[22,65,66] have shown that Jasmonic acid (JA) is associated only to the establishment of the incompatible interaction on this pathosystem. JA synthesis begins in plastids with the dioxygenation of fatty acids in reactions catalyzed by 13-lipoxygenases (13-LOXs), followed by the sequential action of allene oxide synthase (AOS) and allene oxide cyclase (AOC), resulting in the synthesis of 12-oxophytodienoic acid (OPDA). This compound then travels via the cytosol to the peroxisome where it suffers reduction by oxophytodienoate redutase 3 (OPR3) and then several rounds of β-oxidation to form JA[67]. In Trincadeira all of the described enzymes coding genes were down-regulated after *P.viticola* inoculation[65]. In the present work, we have shown that the phosphatidylcholine (PC) content in C18:3 decreased at 6hpi and that the total C18:3 content decreased at 24hpi (Table 4). PC, is a membrane phospholipid that besides providing a structural support is a substrate for signaling molecules such as PA, PI, oxylipins and FFA. PC is hydrolyzed under stress conditions, by phospholipases, promoting PA biosynthesis and free FA (FFA) release[58,68,69]. C18:3 is a substrate required for JA biosynthesis, allowing the increase of JA levels under stress conditions[70]. Thus, our results corroborate previous studies and the hypothesis that JA signaling is not established in the compatible interaction. The decrease of both C18:3 at 24hpi and C18:3/C18:2 ratio at 12 and 24hpi may be related to lipid peroxidation events due to oxidative stress[71].

5.2. Pathogen-driven carbohydrate modulation

In control leaves the diurnal variation in non-structural carbohydrates (NSC) is observed, with a peak close to the end of the light period (12 hpi) when NSC content attained 298.89 ± 10.16 mg g^{-1} DW (Table 5). At the beginning of the light period (24 hpi) the content in NSC decreased.

In inoculated leaves, the highest content of NSS is achieved in the middle of the day (6 hpi), together with the highest SS/starch ratio (2.74 ± 0.39), caused by a strong increase in reducing sugars (not more sucrose or less starch). Starch content is maximum in inoculated leaves at the end of the light period (Table 5).

The first hours upon inoculation are crucial for the establishment of either a compatible or incompatible interaction. Activation of defense responses upon pathogen infection is usually accompanied by a rapid induction of sink metabolism, possibly to satisfy the increased demand for carbohydrates as an energy source to sustain the cascade of cost-intensive direct defense responses[72]. Correspondingly, the formation of the haustorium in the first hours of infection also requires an adequate nutrient supply[73]. Both of these processes require high levels of glucose, and may explain the differences that were found in the NSS as early as 6 hpi. Moreover, no significant differences in photosynthetic pigments concentration were found during the first 24h of infection that suggest photosynthesis variation (Figure 7), thus the NSS variations are probably not linked to pathogen-driven fluctuations in photosynthesis. The elevated concentration of NSS in infected leaves may be associated to an lower consumption of reducing sugar and/or by a lower export of sugars from the leaves (source organs) to other sink tissues[74,75]. In either case, an accumulation of hexoses over the course of the day may lead to an accumulation of photoassimilated carbon in the chloroplasts and metabolized in transitory starch during the day, being hydrolyzed to sustain leaf metabolism and sucrose export during the dark period[76]. Such variations might substantiate our higher accumulation of starch 12 hpi, and also explain why there are no differences relative to control leaves after 24 hpi (end of dark period). This idea is in accordance with other studies that report carbohydrate accumulation in highly colonized leaves[77] with local source-to-sink transition[78,79].

5.3. Alkaloids metabolism

Alkaloids are a large and structurally diverse group of natural products having only in common a ring structure and the presence of a basic nitrogen atom[49]. These compounds can be found in bacteria, fungi, animals and plants[49,50]. Within these kingdoms, multiple biological roles have been attributed to alkaloids, but the most relevant are related to self-preservation of the organism, inhibition of competitors and communication[49]. In the current work, several putative alkaloids were identified at 12 and 24 hpi, usually down accumulated, with the exception of 2 masses at 24 hpi (Appendix 2). One of them (347.11690 m/z (ESI-)) among the possible

putative annotation, Nitidine and Chelerythrine are found (Appendix 2), interestingly, both of these compounds have described anti-parasitic properties[50,80,81].

5.4. ROS signaling in compatible interaction

ROS play an important role as signaling molecules in the regulation of numerous biological processes such as growth, development, and responses to biotic and/or abiotic stimuli in plants[82]. Concerning pathogen resistance, ROS can have a direct role strengthening host cell walls via cross-linking of glycoproteins, lipid peroxidation and activation of ROS-signaling networks. Further regulatory functions have been attributed to ROS in pathogen resistance, especially in conjunction salicylic acid and nitric oxide[83].

In the present work, the accumulation of ROS upon pathogen infection is especially significant at 6 and 12 hpi, suggesting recognition of the pathogen. Nevertheless, ROS accumulation is not sufficient to trigger oxidative burst and set in motion an appropriate defense response.

Compared to a resistant cultivar, which demonstrate a clear oxidative burst, the accumulation of ROS is marginable[22], suggesting that Trincadeira lacks a *P. viticola*-specific recognition system that enables the activation of a successful defense mechanism.

6. Conclusion

In the present work the metabolomic changes of grapevine leaves, in the compatible interaction with *P. viticola*, were characterized. Untargeted metabolomics approach using a FTICR-MS analysis shows distinct metabolic profiles between control and inoculated leaves in the early hours of infection. Multiple metabolite classes exhibit variation in the first hours of infection, being Lipids who displays the most variation, but also Carbohydrates and Alkaloids.

The high percentage of lipids differences, compared to other classes of metabolites, is mainly due to Fatty acids and Flavonoids variations and our analysis by GC and qPCR supports this information, showing variation in fatty acids concentration and in flavonoids biosynthesis pathway as early as 6 hpi. Carbohydrates also appear to have an important role in pathogenesis suggesting pathogen-driven modulation of the carbohydrates metabolism.

7. Bibliography

1. McGovern, P. E., Glusker, D. L., Exner, L. J. & Voigt, M. M. Neolithic resinated wine. *Nature* 480–481 (1996). doi:doi:10.1038/381480a0
2. Organization of Vine and Wine. *2017 OIV Statistical Report on World Vitiviniculture*. (2017).
3. Gessler, C., Pertot, I. & Perazzolli, M. *Plasmopara viticola* : a review of knowledge on downy mildew of grapevine and effective disease management. *Phytopathol. Mediterr.* **50,** 3–44 (2011).
4. Buonassisi, D. *et al.* Breeding for grapevine downy mildew resistance: a review of "omics" approaches. *Euphytica* **213,** 103 (2017).
5. Armijo, G. *et al.* Grapevine Pathogenic Microorganisms: Understanding Infection Strategies and Host Response Scenarios. *Front. Plant Sci.* **7,** (2016).
6. Kamoun, S. *et al.* The Top 10 oomycete pathogens in molecular plant pathology. *Mol. Plant Pathol.* **16,** 413–434 (2015).
7. Madden, L. V., Ellis, M. A., Lalancette, N., Hughes, G. & Wilson, L. L. Evaluation of a Disease Warning System for Downy Mildew of Grapes. *Plant Dis.* **84,** 549–554 (2000).
8. Polesani, M. *et al.* General and species-specific transcriptional responses to downy mildew infection in a susceptible (*Vitis vinifera*) and a resistant (*V. riparia*) grapevine species. *BMC Genomics* **11,** 117 (2010).
9. Legay, G. *et al.* Identification of genes expressed during the compatible interaction of grapevine with *Plasmopara viticola* through suppression subtractive hybridization (SSH). *Eur. J. Plant Pathol.* **129,** 281–301 (2011).
10. Milli, A. *et al.* Proteomic analysis of the compatible interaction between *Vitis vinifera* and *Plasmopara viticola*. *J. Proteomics* **75,** 1284–1302 (2012).
11. Batovska, D. I. *et al.* Biomarkers for the prediction of the resistance and susceptibility of grapevine leaves to downy mildew. *J. Plant Physiol.* **166,** 781–785 (2009).
12. Becker, L. *et al.* Metabolic study of grapevine leaves infected by downy mildew using negative ion electrospray – Fourier transform ion cyclotron resonance mass spectrometry. *Anal. Chim. Acta* **795,** 44–51 (2013).

13. Ali, K. *et al.* Alterations in grapevine leaf metabolism upon inoculation with *Plasmopara viticola* in different time-points. *Plant Sci.* **191–192,** 100–107 (2012).
14. Chitarrini, G. *et al.* Identification of Biomarkers for Defense Response to *Plasmopara viticola* in a Resistant Grape Variety. *Front. Plant Sci.* **8,** (2017).
15. Polesani, M. *et al.* cDNA-AFLP analysis of plant and pathogen genes expressed in grapevine infected with *Plasmopara viticola*. *BMC Genomics* **9,** 142 (2008).
16. Perazzolli, M. *et al.* Downy mildew resistance induced by Trichoderma harzianum T39 in susceptible grapevines partially mimics transcriptional changes of resistant genotypes. *BMC Genomics* **13,** 660 (2012).
17. Vannozzi, A., Dry, I. B., Fasoli, M., Zenoni, S. & Lucchin, M. Genome-wide analysis of the grapevine stilbene synthase multigenic family: genomic organization and expression profiles upon biotic and abiotic stresses. *BMC Plant Biol.* **12,** 130 (2012).
18. Rossin, G. *et al.* Grapevine Downy Mildew *Plasmopara viticola* Infection Elicits the Expression of Allergenic Pathogenesis-Related Proteins. *Int. Arch. Allergy Immunol.* **168,** 90–95 (2015).
19. Guillier, C. *et al.* Toward the Identification of Two Glycoproteins Involved in the Stomatal Deregulation of Downy Mildew–Infected Grapevine Leaves. *Mol. Plant. Microbe Interact.* **28,** 1227–1236 (2015).
20. Perazzolli, M., Palmieri, M. C., Matafora, V., Bachi, A. & Pertot, I. Phosphoproteomic analysis of induced resistance reveals activation of signal transduction processes by beneficial and pathogenic interaction in grapevine. *J. Plant Physiol.* **195,** 59–72 (2016).
21. Gaspero, G. D., Cipriani, G., Adam-Blondon, A.-F. & Testolin, R. Linkage maps of grapevine displaying the chromosomal locations of 420 microsatellite markers and 82 markers for R-gene candidates. *Theor. Appl. Genet.* **114,** 1249–1263 (2007).
22. Figueiredo, A. *et al.* Specific adjustments in grapevine leaf proteome discriminating resistant and susceptible grapevine genotypes to *Plasmopara viticola*. *J. Proteomics* **152,** 48–57 (2017).
23. Figueiredo, A. *et al.* Cultivar-specific kinetics of gene induction during downy mildew early infection in grapevine. *Funct. Integr. Genomics* **12,** 379–386 (2012).

24. Hamiduzzaman, M. M., Jakab, G., Barnavon, L., Neuhaus, J.-M. & Mauch-Mani, B. β-Aminobutyric Acid-Induced Resistance Against Downy Mildew in Grapevine Acts Through the Potentiation of Callose Formation and Jasmonic Acid Signaling. *Mol. Plant. Microbe Interact.* **18,** 819–829 (2005).
25. Kortekamp, A. Expression analysis of defence-related genes in grapevine leaves after inoculation with a host and a non-host pathogen. *Plant Physiol. Biochem.* **44,** 58–67 (2006).
26. Trouvelot, S. *et al.* A β-1,3 Glucan Sulfate Induces Resistance in Grapevine against *Plasmopara viticola* Through Priming of Defense Responses, Including HR-like Cell Death. *Mol. Plant. Microbe Interact.* **21,** 232–243 (2008).
27. Sumner, L. W., Lei, Z., Nikolau, B. J. & Saito, K. Modern plant metabolomics: advanced natural product gene discoveries, improved technologies, and future prospects. *Nat. Prod. Rep.* **32,** 212–229 (2015).
28. Witting, M. *et al.* DI-ICR-FT-MS-based high-throughput deep metabotyping: a case study of the Caenorhabditis elegans–Pseudomonas aeruginosa infection model. *Anal. Bioanal. Chem.* **407,** 1059–1073 (2015).
29. Kortekamp, A. *et al.* Identification, isolation and characterization of a CC-NBS-LRR candidate disease resistance gene family in grapevine. *Mol. Breed.* **22,** 421–432 (2008).
30. Maia, M. *et al.* Metabolite extraction for high-throughput FTICR-MS-based metabolomics of grapevine leaves. *EuPA Open Proteomics* **12,** 4–9 (2016).
31. Suhre, K. & Schmitt-Kopplin, P. MassTRIX: mass translator into pathways. *Nucleic Acids Res.* **36,** W481–W484 (2008).
32. Xia, J. & Wishart, D. S. Using MetaboAnalyst 3.0 for Comprehensive Metabolomics Data Analysis. in *Current Protocols in Bioinformatics* (John Wiley & Sons, Inc., 2002). doi:10.1002/cpbi.11
33. Kanehisa, M., Sato, Y., Kawashima, M., Furumichi, M. & Tanabe, M. KEGG as a reference resource for gene and protein annotation. *Nucleic Acids Res.* **44,** D457–D462 (2016).
34. Ogata, H. *et al.* KEGG: Kyoto Encyclopedia of Genes and Genomes. *Nucleic Acids Res.* **27,** 29–34 (1999).
35. Sud, M. *et al.* LMSD: LIPID MAPS structure database. *Nucleic Acids Res.* **35,** D527–D532 (2007).

36. Nakamura, Y. *et al.* KNApSAcK Metabolite Activity Database for Retrieving the Relationships Between Metabolites and Biological Activities. *Plant Cell Physiol.* **55,** e7–e7 (2014).
37. Vandesompele, J. *et al.* Accurate normalization of real-time quantitative RT-PCR data by geometric averaging of multiple internal control genes. *Genome Biol.* **3,** research0034.1-research0034.11 (2002).
38. Hellemans, J., Mortier, G., De Paepe, A., Speleman, F. & Vandesompele, J. qBase relative quantification framework and software for management and automated analysis of real-time quantitative PCR data. *Genome Biol.* **8,** R19 (2007).
39. Monteiro, F., Sebastiana, M., Pais, M. S. & Figueiredo, A. Reference Gene Selection and Validation for the Early Responses to Downy Mildew Infection in Susceptible and Resistant *Vitis vinifera* Cultivars. *PLOS ONE* **8,** e72998 (2013).
40. Bligh, E. G. & Dyer, W. J. A Rapid Method of Total Lipid Extraction and Purification. *Can. J. Biochem. Physiol.* **37,** 911–917 (1959).
41. Matos, A. R. *et al.* Effects of progressive drought stress on the expression of patatin-like lipid acyl hydrolase genes in Arabidopsis leaves. *Physiol. Plant.* **134,** 110–120 (2008).
42. Lichtenthaler, H. K. Chlorophylls and carotenoids: Pigments of photosynthetic biomembranes. *Methods Enzymol.* **148,** 350–382 (1987).
43. Guy, C. L., Huber, J. L. A. & Huber, S. C. Sucrose Phosphate Synthase and Sucrose Accumulation at Low Temperature. *Plant Physiol.* **100,** 502–508 (1992).
44. Almeida, A. M. *et al.* Responses to water withdrawal of tobacco plants genetically engineered with the AtTPS1 gene: a special reference to photosynthetic parameters. *Euphytica* **154,** 113–126 (2007).
45. Sebastiana, M. *et al.* Oak protein profile alterations upon root colonization by an ectomycorrhizal fungus. *Mycorrhiza* **27,** 109–128 (2017).
46. Childs, R. E. & Bardsley, W. G. The steady-state kinetics of peroxidase with 2,2'-azino-di-(3-ethyl-benzthiazoline-6-sulphonic acid) as chromogen. *Biochem. J.* **145,** 93–103 (1975).
47. Hodges, D. M., DeLong, J. M., Forney, C. F. & Prange, R. K. Improving the thiobarbituric acid-reactive-substances assay for estimating lipid peroxidation in plant tissues containing anthocyanin and other interfering compounds. *Planta* **207,** 604–611 (1999).

48. Walley, J. W., Kliebenstein, D. J., Bostock, R. M. & Dehesh, K. Fatty acids and early detection of pathogens. *Curr. Opin. Plant Biol.* **16,** 520–526 (2013).
49. Cushnie, T. P. T., Cushnie, B. & Lamb, A. J. Alkaloids: An overview of their antibacterial, antibiotic-enhancing and antivirulence activities. *Int. J. Antimicrob. Agents* **44,** 377–386 (2014).
50. Dewick, P. M. Alkaloids. in *Medicinal natural products: a biosynthetic approach* 291–403 (John Wiley & Sons, 2002).
51. Batovska, D. I. *et al.* Biomarkers for the prediction of the resistance and susceptibility of grapevine leaves to downy mildew. *J. Plant Physiol.* **166,** 781–785 (2009).
52. Agati, G. *et al.* Optically-assessed preformed flavonoids and susceptibility of grapevine to *Plasmopara viticola* under different light regimes. *Funct. Plant Biol.* **35,** 77–84 (2008).
53. Yin, X. *et al.* Pathogen development and host responses to *Plasmopara viticola* in resistant and susceptible grapevines: an ultrastructural study. *Hortic. Res.* **4,** hortres201733 (2017).
54. Gamm, M. *et al.* Changes in Carbohydrate Metabolism in *Plasmopara viticola*-Infected Grapevine Leaves. *Mol. Plant. Microbe Interact.* **24,** 1061–1073 (2011).
55. Dai, G. H., Andary, C., Mondolot-Cosson, L. & Boubals, D. Histochemical studies on the interaction between three species of grapevine, *Vitis vinifera*, V. rupestris and V. rotundifolia and the downy mildew fungus, *Plasmopara viticola*. *Physiol. Mol. Plant Pathol.* **46,** 177–188 (1995).
56. Dai, G., Andary, C., Mondolot-Cosson, L. & Boubals, D. Histochemical Responses of Leaves of In Vitro Plantlets of Vitis spp. to Infection with *Plasmopara viticola*. *Phytopathology* **85,** 149 (1995).
57. Gindro, K., Pezet, R. & Viret, O. Histological study of the responses of two *Vitis vinifera* cultivars (resistant and susceptible) to *Plasmopara viticola* infections. *Plant Physiol. Biochem.* **41,** 846–853 (2003).
58. Hou, Q., Ufer, G. & Bartels, D. Lipid signalling in plant responses to abiotic stress. *Plant Cell Environ.* **39,** 1029–1048 (2016).
59. Horn, P. J. & Chapman, K. D. Lipidomics in situ: Insights into plant lipid metabolism from high resolution spatial maps of metabolites. *Prog. Lipid Res.* **54,** 32–52 (2014).

60. Latouche, G., Bellow, S., Poutaraud, A., Meyer, S. & Cerovic, Z. G. Influence of constitutive phenolic compounds on the response of grapevine (*Vitis vinifera* L.) leaves to infection by *Plasmopara viticola*. *Planta* **237,** 351–361 (2013).

61. Gunnaiah, R. & Kushalappa, A. C. Metabolomics deciphers the host resistance mechanisms in wheat cultivar Sumai-3, against trichothecene producing and non-producing isolates of Fusarium graminearum. *Plant Physiol. Biochem.* **83,** 40–50 (2014).

62. Agafonov, A. *et al.* A permeability transition in liposomes induced by the formation of Ca2+/palmitic acid complexes. *Biochim. Biophys. Acta BBA - Biomembr.* **1609,** 153–160 (2003).

63. Mandal, M. K. *et al.* Oleic Acid–Dependent Modulation of NITRIC OXIDE ASSOCIATED1 Protein Levels Regulates Nitric Oxide–Mediated Defense Signaling in Arabidopsis. *Plant Cell Online* **24,** 1654–1674 (2012).

64. Zhang, W. *et al.* The Oleate-Stimulated Phospholipase D, PLDδ, and Phosphatidic Acid Decrease H2O2-Induced Cell Death in Arabidopsis. *Plant Cell Online* **15,** 2285–2295 (2003).

65. Figueiredo, A., Monteiro, F. & Sebastiana, M. First clues on a jasmonic acid role in grapevine resistance against the biotrophic fungus *Plasmopara viticola*. *Eur. J. Plant Pathol.* **142,** 645–652 (2015).

66. Guerreiro, A., Figueiredo, J., Sousa Silva, M. & Figueiredo, A. Linking Jasmonic Acid to Grapevine Resistance against the Biotrophic Oomycete *Plasmopara viticola*. *Front. Plant Sci.* **7,** (2016).

67. Dave, A. & Graham, I. A. Oxylipin Signaling: A Distinct Role for the Jasmonic Acid Precursor cis-(+)-12-Oxo-Phytodienoic Acid (cis-OPDA). *Front. Plant Sci.* **3,** (2012).

68. Testerink, C. & Munnik, T. Molecular, cellular, and physiological responses to phosphatidic acid formation in plants. *J. Exp. Bot.* **62,** 2349–2361 (2011).

69. Blée, E. Impact of phyto-oxylipins in plant defense. *Trends Plant Sci.* **7,** 315–322 (2002).

70. Wasternack, C. & Hause, B. Jasmonates: biosynthesis, perception, signal transduction and action in plant stress response, growth and development. An update to the 2007 review in Annals of Botany. *Ann. Bot.* **111,** 1021–1058 (2013).

71. Matos, A. R. & Pham-Thi, A.-T. Lipid deacylating enzymes in plants: Old activities, new genes. *Plant Physiol. Biochem.* **47,** 491–503 (2009).

72. Wingler, A. & Roitsch, T. Metabolic regulation of leaf senescence: interactions of sugar signalling with biotic and abiotic stress responses. *Plant Biol.* **10,** 50–62 (2008).

73. Divon, H. H. & Fluhr, R. Nutrition acquisition strategies during fungal infection of plants. *FEMS Microbiol. Lett.* **266,** 65–74 (2007).

74. Lemoine, R. *et al.* Source-to-sink transport of sugar and regulation by environmental factors. *Front. Plant Sci.* **4,** (2013).

75. Wardlaw, I. F. Tansley Review No. 27 The control of carbon partitioning in plants. *New Phytol.* **116,** 341–381 (1990).

76. Smith, A. M. & Stitt, M. Coordination of carbon supply and plant growth. *Plant Cell Environ.* **30,** 1126–1149 (2007).

77. Hay, R. K. M. & Walker, A. J. Introduction to the physiology of crop yield. *Introd. Physiol. Crop Yield* (1989).

78. Scholes, J. D., Lee, P. J., Horton, P. & Lewis, D. H. Invertase: understanding changes in the photosynthetic and carbohydrate metabolism of barley leaves infected with powdery mildew. *New Phytol.* **126,** 213–222 (1994).

79. Zadoks, J. C. & Schein, R. D. Epidemiology and plant disease management. *Epidemiol. Plant Dis. Manag.* (1979).

80. Castillo, D., Sauvain, M., Rivaud, M. & Jullian, V. In Vitro and In Vivo Activity of Benzo[c]phenanthridines against Leishmania amazonensis. *Planta Med.* **80,** 902–906 (2014).

81. Jullian, V., Bourdy, G., Georges, S., Maurel, S. & Sauvain, M. Validation of use of a traditional antimalarial remedy from French Guiana, Zanthoxylum rhoifolium Lam. *J. Ethnopharmacol.* **106,** 348–352 (2006).

82. Baxter, A., Mittler, R. & Suzuki, N. ROS as key players in plant stress signalling. *J. Exp. Bot.* **65,** 1229–1240 (2014).

83. Torres, M. A., Jones, J. D. G. & Dangl, J. L. Reactive Oxygen Species Signaling in Response to Pathogens. *Plant Physiol.* **141,** 373–378 (2006).

Appendix 1

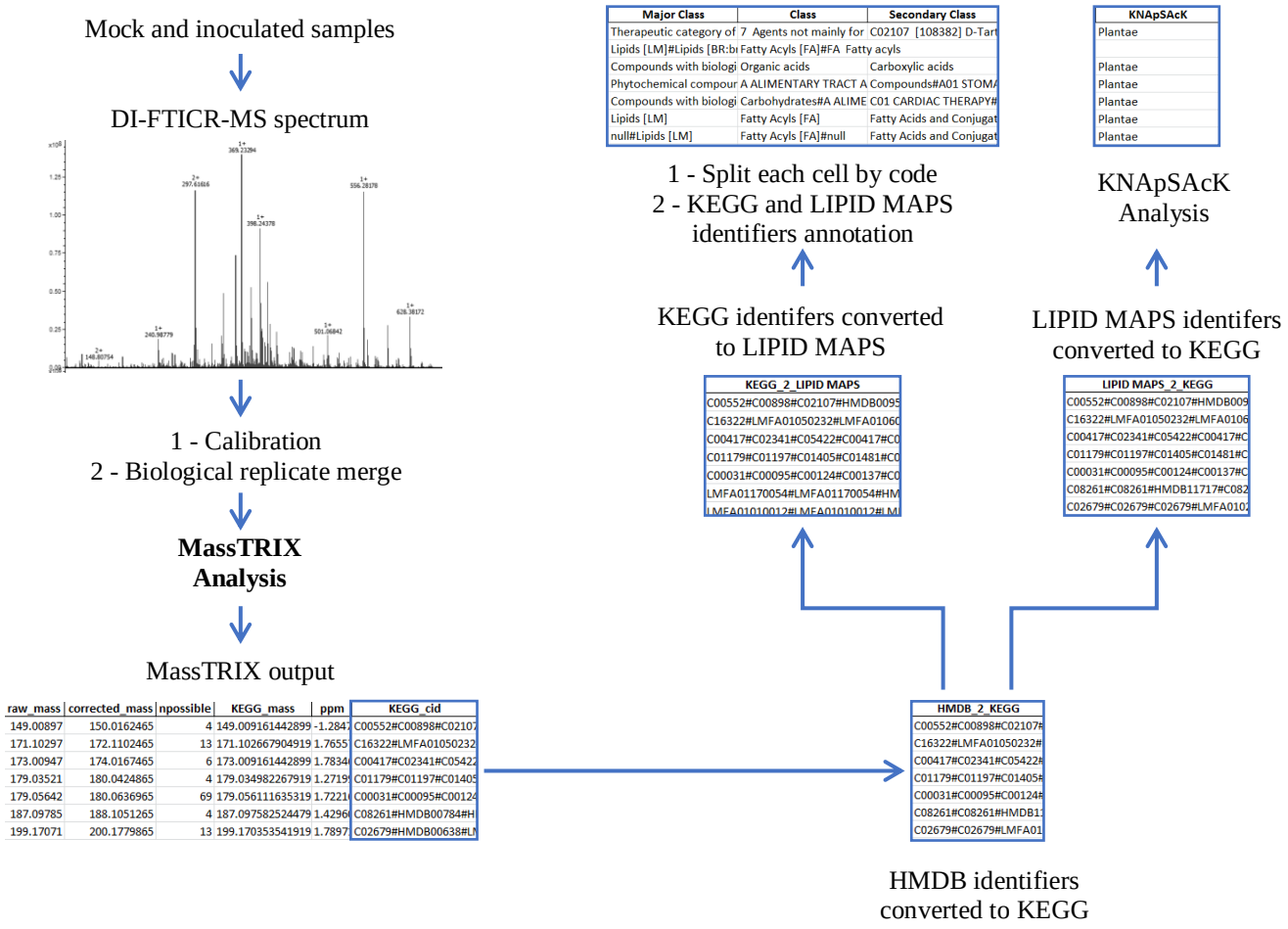

Appendix 1 - Schematic diagram of the automatic pipeline metabolome annotation.

Appendix 2

	Fold Change	p.value	m/z	ESI Mode	KEGG_cid*	Putative ID*	Major Class	Class	KNApSAcK
6 hpi	-4.4	0.018	205.03599	-	C00725	Lipoic acid ([M-H]-)	Lipids	Fatty Acyls	
	9.5	0.006	309.17530	-	LMFA06000114	2-chloropalmitaldehyde ([M+Cl35]-)	Lipids	Fatty Acyls	
	3.0	0.047	329.27001	-	HMDB11533	2-hexadecanoyl-glycerol ([M-H]-)	Lipids	Glycerolipids	
	-8.0	0.021	331.06762	-	C01158	1-O-Galloyl-beta-D-glucose ([M-H]-)	Carbohydrate and derivatives		
	2.5	0.045	339.99039	+	C15249	2-(3,5-Dichlorophenylcarbamoyl) -1,2-dimethylcyclopropane-1-carboxylic acid ([M+K39]+)	Lipids	Polyketides	Plantae
	2.1	0.034	367.35883	-	C08320	Tetracosanoic acid ([M-H]-)	Lipids	Fatty Acyls	Plantae
	20.8	0.001	425.13612	+	LMPK12050212	Ulexone B ([M+Na]+)	Lipids	Polyketides	Plantae
	6.4	0.010	543.13206	+	C00492	Raffinose ([M+K39]+)	Carbohydrates	Oligosaccharides	Plantae
	-5.1	0.046	647.51642	+	LMST01020022	15:1 Cholesteryl ester([M+K39]+)	Lipids	Sterols	
12 hpi	9.8	0.005	425.13602	+	LMPK12050212	Ulexone B ([M+Na]+)	Lipids	Polyketides	Plantae
	3.1	0.033	403.20466	-	LMST04010429	3-Oxochola-1,4,6-trien-24-oic Acid ([M+Cl35]-)	Lipids	Sterols	
	-57.8	0.000	149.00920	-	C00552	meso-Tartaric acid([M-H]-)	Organic acids		Plantae
	-2.0	0.001	377.08619	-	C00089	Sucrose ([M+Cl35]-)	Carbohydrates and derivatives	Oligosaccharides	Plantae
	-3.8	0.002	351.05473	-	LMFA01140024	Majusculoic acid ([M+Cl37]-)	Lipids	Fatty Acyls	

	-2.0	0.004	205.03623	-	C00725	Lipoic acid ([M-H]-)	Lipids	Fatty Acyls	
	-9.1	0.013	297.24299	-	C00869	2-Oxooctadecanoic acid ([M-H]-)	Lipids	Fatty Acyls	Plantae
	-1.7	0.025	388.11876	-	C12201	(+/-)-6-Acetonyldihydrosanguinarine ([M-H]-)	Alkaloid		
	-5.1	0.042	223.08338	-	HMDB04328	Temurin ([M-H]-)	Alkaloid		
	-5.4	0.001	370.03717	+	C01265	3',4',5-Trihydroxy-3,7-dimethoxyflavone ([M+K40]+)	Lipids	Polyketides	Plantae
	-4.4	0.002	356.99768	+	C04478	3-Deoxy-D-manno-octulosonate 8-phosphate ([M+K39]+)	Others		
	-4.0	0.009	362.09710	+	C10632	Acronycine ([M+K41]+)	Phytochemical compounds	Alkaloids	Plantae
	-1.8	0.012	245.00607	+	C01251	(R)-2-Hydroxybutane-1,2,4-tricarboxylate ([M+K39]+)	Organic acids		
	-3.8	0.017	772.27402	+	C16523	3'-N-Debenzoyl-2'-deoxytaxol ([M+K39]+)	Phytochemical compounds	Terpenoids	
	-3.6	0.017	343.12357	+	C00185	Cellobiose ([M+H]+)	Carbohydrates and derivatives	Oligosaccharides	Plantae
	-1.9	0.017	219.02679	+	C04045	3-(3,4-Dihydroxyphenyl)pyruvate ([M+Na]+)	Carbohydrates and derivatives		Plantae
	-4.2	0.019	388.14906	+	C14676	4-Chloroprogesterone ([M+K40]+)	Others		
	-3.0	0.043	395.07417	+	LMPK12060077	Stemonal ([M+Na]+)	Lipids	Polyketides	Plantae
24h	24.8	0.000	425.13632	+	LMPK12050212	Ulexone B ([M+Na]+)	Lipids	Phenylpropanoids	Plantae
	2.9	0.008	617.25395	-	C09999	Aralionine A ([M+Cl35]-)	Alkaloid		Plantae
	2.4	0.016	347.11690	-	C09595	Nitidine ([M-H]-)	Phytochemical compounds	Alkaloids	Plantae

	-3.7	0.004	381.37446	-	HMDB02361	Pentacosanoic acid ([M-H]-)	Lipids	Fatty Acyls	
	-5.9	0.018	473.28250	-	LMST03020391	(17Z)-1alpha,25-dihydroxy-26,27-dimethyl-17,20,22,22,23,23-hexadehydrovitamin D3 / (17Z)-1alpha,25-dihydroxy-26,27-dimethyl-17,20,22,22,23,23-hexadehydrocholecalciferol ([M+Cl35]-)	Lipids	Sterols	
	-6.2	0.022	241.07303	-	C00176	R replaced by H in Flavin ([M-H]-)	Others		Plantae
	-15.7	0.035	339.19448	-	LMFA01050099	2,15,16-trihydroxy palmitic acid ([M+Cl35]-)	Lipids	Fatty Acyls	
	-8.0	0.001	415.21187	+	C10658	Magnoshinin ([M+H]+)	Alkaloids	Phenylpropanoids	Plantae
	-7.3	0.005	437.19373	+	C08076	Sulconazole ([M+K41]+)	Others	Phenylpropanoids	Plantae
	-1.7	0.007	279.15937	+	C03343	2-Ethylhexyl phthalate ([M+H]+)	Lipids	Prenol Lipids	
	-1.5	0.010	347.13399	+	C09771	Aucubin ([M+H]+)	Lipids	Prenol Lipids	Plantae
	-1.5	0.028	365.10548	+	C00089	Sucrose([M+Na]+)	Carbohydrates	Carbohydrates	Plantae
	-2.5	0.034	437.30288	+	C08898	Diosgenin ([M+Na]+)	Lipids	Fatty Acyls	Plantae

Appendix 2 – Different accumulated metabolites, putative identification and classification at 6, 12 and 24 hpi.

Fold Change in inoculated leaves; p.value corresponds to the p-value value observed; m/z is the mass detected by the FTICR-MS; ESI Mode in positive (+) or negative (-) mode; KEGG_cid corresponds to the putative database identifier; Putative ID correspond to the putative identification; Major Class and Class are obtain as depicted in Materials and methods; KNApSAcK indicate if the compound are described in plants on the KNApSAcK database.

* Due to space constrains only the first tentative identification is shown. Complete dataset is presented as digital data.

Appendix 3

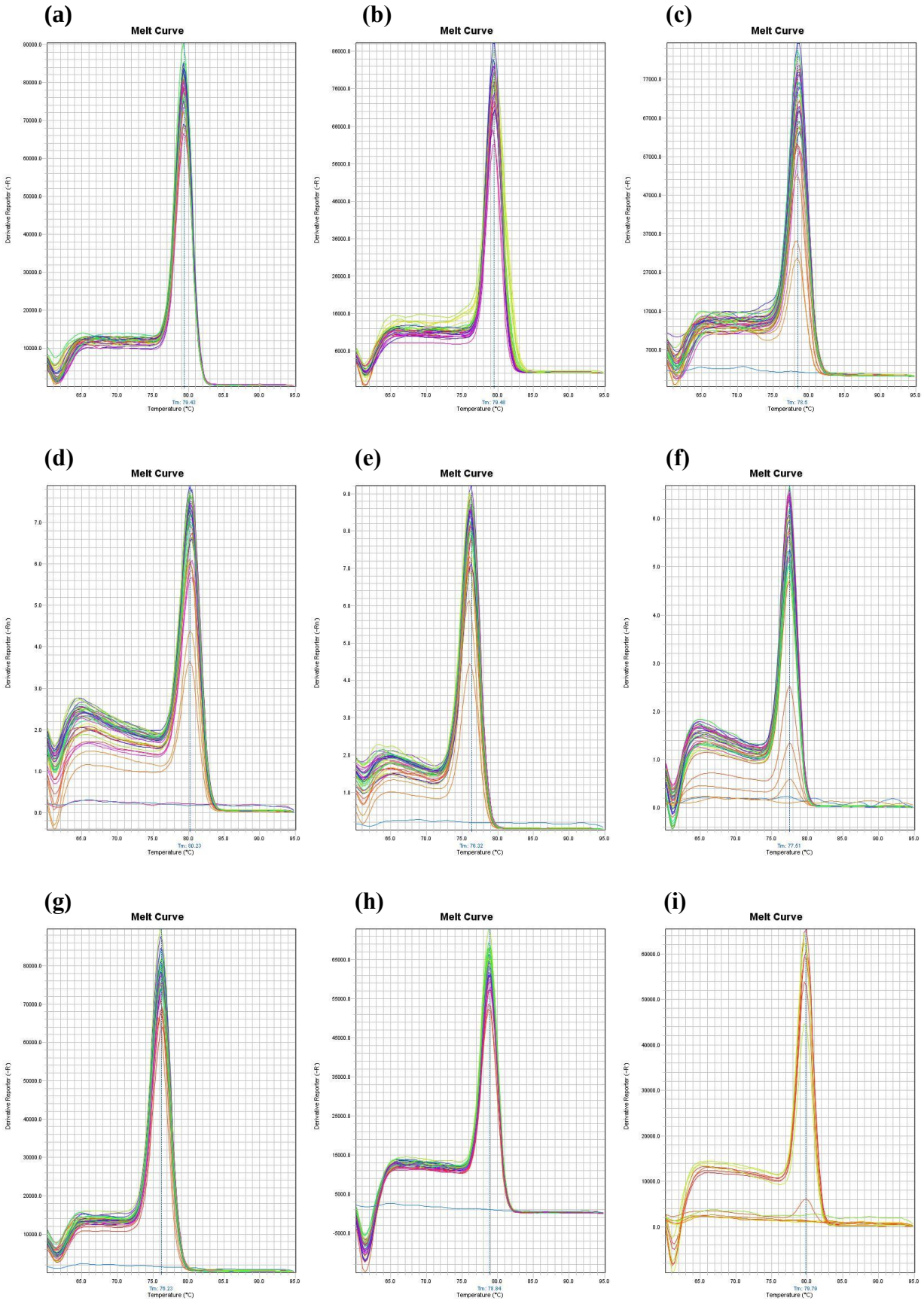
(a)
Melt Curve
(b)
Melt Curve
(c)
Melt Curve
(d)
Melt Curve
(e)
Melt Curve
(f)
Melt Curve
(g)
Melt Curve
(h)
Melt Curve
(i)
Melt Curve
Temperature (°C)

Appendix 3

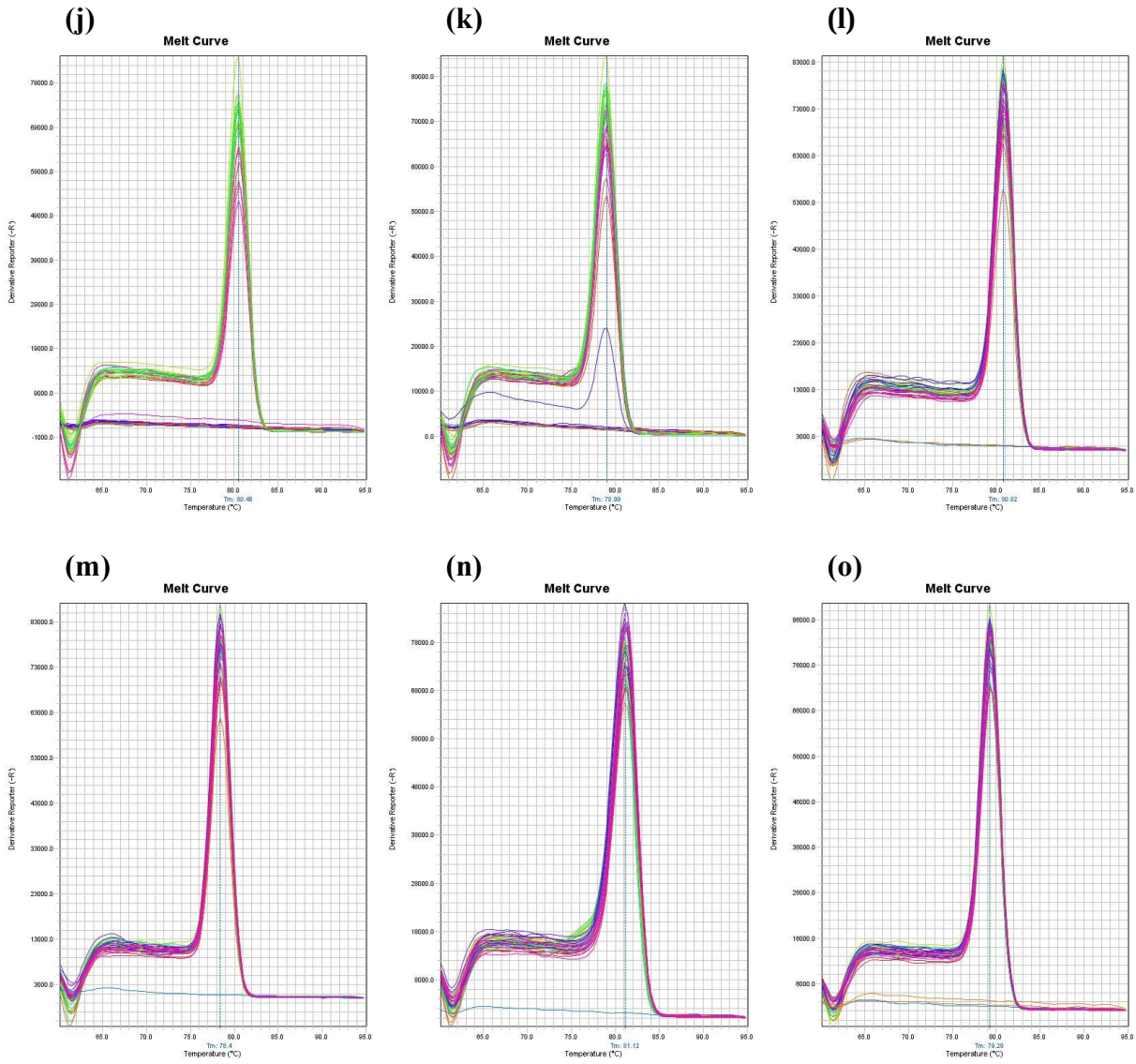

Appendix 3 – Melting curves of targeted genes.

(a) *EF1α*; (b) *TRP7B*; (c) *SAND*; (d) *LAR2*; (e) *ANR*; (f) *FatB*; (g) *FLS-A*; (h) *FLS-B*; (i) *FLS-C*; (j) *FLS-D*; (k) *FLS-E*; (l) *FLS-F*; (m) *F3'5'H*; (n) *DFR*.